

FINAL REPORT

NASA GRANT NAG8-711

**NUCLEATION AND GROWTH CONTROL
IN PROTEIN CRYSTALLIZATION**

Period of Performance
3/14/88 through 9/13/90

Principal Investigator

FRANZ ROSENBERGER
Professor of Physics and Director, CMMR

Co-Investigators

THOMAS A. NYCE
Research Scientist

EDWARD J. MEEHAN
Associate Professor of Chemistry

JENNIFER W. SOWERS
Research Analyst III

LISA A. MONACO
Graduate Research Assistant

Center for Microgravity and Materials Research
University of Alabama in Huntsville
Huntsville, Alabama 35899

Table of Contents

1. Introduction	1
2. Solubility Determinations	1
2.1 Batch technique.....	2
2.2 Scintillation technique	2
2.3 Lysozyme solubilities	3
2.3.1 Solution preparation	3
2.3.2 Solubility data	4
2.4 Canavalin solubilities	5
2.4.1 Solution preparation	5
2.4.2 Solubity data	6
3. Thermostated Solution Cell with Growth Sting	8
3.1 Experimental setup	8
3.2 Growth experiments	9
4. Microscopic Growth Kinetics Studies	10
4.1 Microscopic growth cell	10
4.2 Image storage and processing system	11
4.3 Preliminary results	12
5. Growth Experiments in Thermosyphon Flow	13
5.1 Thermosyphon technique	13
5.2 Results with lysozyme	13
6. Mathematical Model for Concentration Distribution in Hanging Drop at Low Gravity	14
7. Summary	14
8. References	15
9. Figure Captions and Figures	16
10. Presentations and Publications of Research under this Grant	42
11. Attachments	43

1. Introduction

In this final report we summarize the work performed under NASA Grant NAG8-711 during the period March 14, 1988 through September 13, 1990, which includes a six-months no-cost extension. The objectives of this work were:

1. Development of a technique for the expedient, semi-automated determination of protein solubilities as a function of temperature. Application of this technique to proteins other than lysozyme.
2. Development of a small solution cell with adjustable temperature gradients for the growth of proteins at a predetermined location through temperature programming.
3. Development of a microscopy system with image storage and processing capability for high resolution optical studies of temperature controlled protein growth and etching kinetics.
4. Conclusion of the growth experiments with lysozyme in a thermosyphon flow arrangement that was begun under NASA Grant NAG8-098.
5. Development of a mathematical model for the evolution of evaporation/diffusion induced concentration gradients in the hanging drop protein crystallization technique.

In the following we summarize these activities and discuss the results obtained. At the end of the report we list the various presentations and publications that have resulted from this work.

2. Solubility Determinations

Current protein crystallization practices provide for little control of the actual nucleation and growth processes [1]. In contrast to standard practice in inorganic crystal growth, nucleation and growth stages of protein crystallization are typically not separated [1,2] and, hence, too many and too small crystals are obtained in most attempts. Recently, however, the temperature dependence of the solubility of some proteins has been studied in this group [3] and other groups [4,5]. Such data provide, for the first time, the possibility to conduct protein crystallization experiments in a controlled and kinetically advantageous way [1]. After a summary of the batch technique for solubility measurements [3] in Sect. 2.1, we will describe in Sect. 2.2 a simple scintillation (light scattering) technique for semi-automated solubility data determinations that we have developed in continuation of our feasibility studies with large volumes of lysozyme solutions [2]. In Sects. 2.3 and 2.4 we report and discuss solubility data for lysozyme and canavalin, respectively, obtained by these techniques.

2.1 Batch Technique

Parallel to the development of the scintillation technique (see Sect. 2.2), we have continued to apply the batch technique for solubility determinations. In particular we concentrated on lysozyme in the 20-30°C range, where our earlier measurements [3] indicated more or less apparent maxima in solubility depending on the salt concentration. The technique was described in detail in [3]. In essence, it consisted in the long-time storage (up to 10 months) of carefully prepared solutions (1 ml) at various defined temperatures. The equilibration process between solid and solution was periodically checked by UV absorption. The structure of the crystals that formed in equilibrium with the solutions (tetragonal vs. orthorhombic for lysozyme) were judged from their habit.

2.2 Scintillation Technique

Figure 1 gives a schematic presentation of the experimental setup for solubility determinations using optical scintillation. The carefully purified protein solution (see Sects. 2.3.1 and 2.4.1) is placed in a jacketed fluorimeter cell that is connected to a constant temperature bath. The temperature of the solution in the cell is monitored by a three-lead thermistor inserted into an opening of the cell. A magnetic stirring motor continuously drives a magnetic stir flea in the cell. A laser beam is directed through the solution. When the solution is clear, the beam is only slightly scattered by the solution itself as well as by foreign particulates. Upon nucleation and growth of crystallites, the intensity of the scattered light increases markedly. The scattered light is collected by a lens and focused on a photodiode. Amplified photodiode and thermistor outputs are connected via a MacADIOS Model 411 interface to a MacIntosh Plus computer for data acquisition and generation of control outputs. A solid state relay connected to the MacADIOS 411 controls a motor that drives the temperature set point on the circulating water bath.

A "typical" experiment with a protein solution of approximately known behavior is conducted as follows. The temperature of the cell is set to room temperature. After centrifugation and concentration determination (as described later), the protein solution is loaded into the cell. At this point the data acquisition program is operating. The temperature of the bath, and thus of the cell, is then lowered (or raised for retrograde solubility) appropriately to induce nucleation. Once nucleation occurs and the diode signal approaches saturation (as observed on the computer screen and by the turbidity of the solution) the temperature of the cell is increased to approximately 3-5°C below (or above, for retrograde solubility) the expected solubility temperature. The computer program instigates further incremental temperature changes at fixed time intervals by controlling the set point of the water bath. As the solubility temperature is approached for a given protein concentration, the number of scattering crystallites diminishes and hence, the diode signal decreases. Once the

scattered light intensity has decreased below the diode saturation value, each further temperature increment causes the diode signal to first decrease relatively rapidly and then to level out at a new reduced intensity that corresponds to the equilibrium concentration of crystallites at that new temperature. This "scalping" of the signal associated with temperature changes is illustrated by Fig. 2 obtained with lysozyme. This change in slope reflects, of course, the dissolution kinetics of the specific protein. Upon dissolution of the last crystallites, the diode signal returns to the baseline and further temperature changes do not result in a change in the diode signal; see Figs. 2-4.

The scintillation technique for solubility determinations has advantages over other methods used previously [3,5]. It allows for rapid data acquisition since the nucleation and dissolution times are minimized by the continuous stirring of the solution. Furthermore, with the scintillation method one can readily determine a "working range" for temperature-controlled crystal growth experiments. Also, this technique does not require the packing of microcolumns with protein crystals with which the solution is to be equilibrated [5]. Though the application of the scintillation technique to lysozyme (Figs. 2-5 and Sect. 2.2.2) proved optimal, later experiments with canavalin (Sect. 2.3.2) and horse serum albumin (to be reported under Grant NAG8-824) revealed some limitations. Denatured protein can cause erroneous readings. Multiple crystalline forms can also confuse the results. Furthermore, data can be difficult to obtain if the crystallites of a material do not scatter a sufficient amount of light, i.e. the crystallites' refractive index closely matches that of the solution. Also, this technique is, of course, not able to determine temperature-independent solubilities of materials.

2.3 Lysozyme Solubilities

2.3.1 Solution preparation

Lysozyme chloride from chicken egg white, Grade VI (L2879, 90% protein, 5% NaCl) was purchased from Sigma Chemical Company. The protein was dissolved in deionized water at room temperature. The solution was filtered with a glass fiber filter using a Buchner funnel and vacuum flask and then with a Nalgene sterile (0.4 μm) filter. To remove salts from the protein solution, the filtrate was dialyzed against deionized water for a total of 30 hours. In prior dialysis experiments with NaCl solutions of known concentrations, employing a Na^+ specific electrode, we had established that 25 hours of dialysis with two changes of diH_2O are sufficient for complete salt removal.

The protein was then dialyzed against 0.05M acetate buffer, pH 4.5, 0.01% NaN_3 for a total of 60 hours. During this time the reservoir was periodically replaced with fresh buffer solution. After the dialysis, the lysozyme solution was filtered using a Nalgene sterile (0.4 μm) filter and concentrated using an Amicon ultrafiltration apparatus. The pH of the protein

solution was checked with an Orion SA 520 pH meter. The concentration of lysozyme was calculated (using Beer's Law, $A = \epsilon l C$ and assuming $\epsilon_{1\%}$, $280 \text{ nm} = 26.4$) upon measuring the solution's absorbance at 280 nm with a Beckman DU-68 spectrophotometer. This lysozyme stock solution was stored at 4°C.

For the "batch" lysozyme solubility studies, stock solutions of 0.05M acetate buffer, pH 4.5, 0.01% NaN_3 and of NaCl in 0.05M acetate buffer, pH 4.5, 0.01% NaN_3 were prepared. Solutions with predetermined protein concentrations and salt concentrations were then obtained by adding appropriate volumes of the stock solutions. These various protein solutions were pipetted into sterile 5 ml test tubes. The tubes were sealed and placed in temperature baths at 20°, 22°, 24°, 25°, 26°, 28°, and 30°C.

For each scintillation experiment with lysozyme, appropriate amounts of the stock protein, buffer, and salt solutions were mixed. The resulting solution was centrifuged at 9,000-10,000 rpm in a Savant microcentrifuge to remove dust and/or particulate matter. The lysozyme concentration was obtained using absorbance readings obtained with a Beckman DU-68 spectrophotometer and using Beer's law. At the conclusion of each experiment, the lysozyme concentration was again determined by measuring the absorbance.

2.3.2 *Lysozyme solubility data*

Figure 5 gives a comparison of lysozyme solubility data obtained by our scintillation technique and those data recently obtained by Pusey [6] with the equally rapid packed micro-column technique [5]. Agreement is obtained within the experimental errors. On the other hand, rather poor agreement between scintillation and batch data was obtained. This is evident from Fig. 6 in which the 3.0% NaCl scintillation data from Fig. 5 and 2.1% NaCl scintillation data are compared with a few corresponding solubility data obtained by the batch method. For tetragonal lysozyme crystals the "batch solubility" at 2.5% and 3.0% NaCl exceeds that obtained by scintillation significantly; although both techniques reflect a decrease in solubility with increasing salt concentration. The batch data for orthorhombic lysozyme will be discussed later.

There are several possibilities for the differences in solubility values obtained from the two methods. One must remember that the batch experiments required up to 10 months before the concentration of the unstirred solutions, as determined by UV absorption, acquired some steady value. During such a long time it is difficult to maintain constant temperatures (power failures?), avoid bacterial contaminations, and evaporation from the test tubes. Conversely each solution placed in the scintillation cell was freshly prepared, the temperature was monitored during the entire experiment with 0.1 °C resolution, and the absorbance measurements were carried out with a spectrophotometer which is calibrated prior to each measurement.

However, the batch experiments shed considerable light on the nature of the apparent solubility maximum for lysozyme found earlier [3]. The data shown in Figs. 7-10 show unambiguously that the solubility for orthorhombic lysozyme crystals, which are more stable than tetragonal crystals at higher temperatures, is considerably less than that for tetragonal lysozyme solubility at all temperatures and salt concentrations investigated. Solutions with salt concentrations above 3.0% more often produced tetragonal crystals rather than orthorhombic crystals. Very interestingly, in several of the solutions, tetragonal crystals formed first, but later the crystals converted to the orthorhombic form. Solutions with both forms present displayed again the "retrograde" solubility range above 24°C observed earlier [3]. This can now be understood in terms of a superposition of the different solubilities, where the specific (declining value) of the solubility found is subject to the equilibration kinetics of the two forms.

The lysozyme solubility data obtained for the tetragonal form with the scintillation technique are summarized in Fig. 11. Since the technique requires a decrease in temperatures between 0° to 10°C to induce lysozyme nucleation within a short time (one to three hours) the formation of tetragonal rather than orthorhombic crystals is much more likely. Solubility curves were obtained using the scintillation technique for lysozyme at 2.1%, 2.5%, and 3.0% NaCl. All lysozyme solubility curves resulting from the scintillation method resemble each other in shape and slope, with the solubility clearly decreasing with increasing salt concentration.

In summary, we feel that the scintillation technique, which readily yields considerably less scattered data on much smaller volumes than the batch technique [3] and which is in good agreement with the microcolumn technique [5], can be considered as a mature method for determinations of temperature-dependent (protein) solubilities. Further efforts will concentrate on a miniaturization of the technique in order to facilitate its application to protein solutions that, for economic reasons, permit only small solution volumes.

2.4 *Canavalin solubilities*

2.4.1 *Solution preparation*

Canavalin was isolated from Jack Bean meal (Sigma J-0125, Lot 37F-3720) using the isolation procedure of Smith et al. [1]. Canavalin was also received from Prof. McPherson, University of California at Riverside. Isoelectric focusing (IEF) polyacrylamide gel electrophoresis (PAGE) was utilized to follow the isolation steps and to determine the number of constituents in the final canavalin solutions. The gels illustrated the presence of subsequently fewer components in the solutions after each successive isolation step. The canavalin from McPherson was also subjected to IEF/PAGE and compared to the canavalin isolated in our laboratory. Samples from both isolations migrated to the same relevant

position on the gel. Clear bands were not obtained, however, as each sample demonstrated "spreading." This spreading could be due to the conditions under which the gel was run or to the presence of other proteins. All canavalin was stored at -20°C .

For our solubility studies with the batch technique, solutions were prepared as follows. The frozen material was thawed at room temperature and centrifuged to remove excess liquid. The crystalline material was then "washed" with filtered, deionized water (canavalin is insoluble in water) and centrifuged again. To dissolve the canavalin pellet, 0.05M phosphate buffer, pH 8.0, 1.33% NaCl, 0.01% NaN_3 was added. After centrifugation the canavalin supernatant was removed and the pH was determined with pH paper to be 5.5 to 6.0. (These experiments were performed before acquisition of a pH micro-electrode). A stock solution of NaCl in 0.05M phosphate buffer, pH 6.1, 0.01% NaN_3 was prepared. Triplicate sets of canavalin solutions containing NaCl concentrations of 0.5%, 0.75%, 1.0%, 2.0%, 5.0%, 10.0%, 15.0%, and 20.0% were prepared in small, 2 ml glass vials with screw tops. The initial pH of all solutions was 5.5-6.0.

2.4.2 Canavalin solubility data

We first attempted to use Pusey and Gernert's "two-column micro-solubility method" [5] to study the solubility of canavalin. However, we encountered problems such as pronounced bacterial contamination and crystal degradation. Since canavalin was initially believed to have strong temperature-dependent solubility, we also tried to use the scintillation technique to develop a solubility diagram. Again, this approach was continuously plagued by problems. The nucleation/dissolution response was so slow that, even with seeding, a typical canavalin experiment required from 3-5 days to complete. A typical, poor response of a canavalin solution in the scintillation cell is shown in Fig. 12. Although crystallites were present, the scattered light intensity was low, with the maximum photodiode signal received being typically only 15% of the photodiode saturation limit. This can be seen from Fig. 12 in comparison with the corresponding Figs. 2-4 for lysozyme. Furthermore, upon microscopic observation of the crystallites, bacterial contamination was observed. Due to these problems, the study of canavalin solubility using the scintillation technique was aborted.

However, interesting results on the canavalin solubility were obtained with the batch technique. A set of solutions was prepared as described above and stored at 4°C , 10°C , and 20°C . At two week intervals the canavalin concentration was determined using UV absorption ($\epsilon_{1\%}^{1\text{cm}}_{280\text{nm}}=6.8$), and the pH of all solutions was measured with an Orion SA 520 meter and a pH microelectrode. After eight weeks, the solutions seemed to have equilibrated. At all temperatures crystals were present at 0.5%, 0.75%, and 1.0% NaCl; in 2.0% NaCl solutions crystals formed only at 4°C . The solutions with NaCl concentrations

greater than 2.0% contained no crystals. The crystals were flat and rectangular, unlike the rhombohedrals that we expected based on reported crystallization conditions [4,7,8]. We found that, as observed earlier [7,8], in the solutions where crystals formed, the pH had significantly increased (see Table 1), although the solutions were buffered at an initial pH of 5.5. Though it has been suggested that upon crystallization, hydrogen ions are incorporated into the crystal [4], the exact mechanism for this pH increase is not understood as yet.

Table 1: Final pH values of canavalin solutions that were initially buffered to pH=5.5-6

%NaCl	4°C	10°C	20°C
0.5	6.60	6.57	6.50
0.75	6.52	6.50	6.43
1	6.49	6.45	6.39
2	6.39	6.34	6.29
5	6.16	6.14	6.12
10	5.95	5.92	5.92
15	5.79	5.76	5.74
20	5.66	5.64	5.63

Bold numbers indicate presence of crystals

Figures 13 and 14 summarize the data obtained in this first series of experiments for the dependence of the canavalin equilibrium solubility on temperature and NaCl concentration, respectively. One sees that canavalin has a "normal" temperature dependence of its solubility. The solubility values are somewhat higher than those reported by DeMattei and Feigelson [4]. Three possible reasons may be: the solutions had not thoroughly equilibrated; this crystal form of canavalin has higher solubility than the expected rhombohedral form; contaminating proteins from the lengthy isolation procedure may have been present. Note from Fig. 14 that the canavalin solubility increases with an increase in NaCl concentration. This trend is opposite to that of lysozyme.

A second group of batch experiments was conducted with several parameters chosen differently. A different batch of canavalin was used (obtained from McPherson), ammonium hydroxide was used to initially dissolve the material, and the initial pH was adjusted with acetic acid to 6.5. The NaCl concentrations in these experiments were 0.5%, 0.75%, 1.0%, 2.0%, and 5.0%. Solutions were stored at 10°C and 20°C. Crystals formed in all solutions at

10°C within 24 hours. Also, in the 0.5% and 0.75% NaCl solutions crystals formed at 20°C within 24 hours. The crystals at 10°C initially appeared to be the same flat, rectangular crystals as observed in the previous experiment; but at the end of the experiment, only rhombohedral crystals were observed in these vials. The crystals grown at 20°C were clearly rhombohedral. The solubility data for the 10°C samples are displayed in Fig. 15. The 20°C experiments were aborted due to bath failure. Note that the solubilities obtained from this batch with higher pH values are much lower than found in the first set of experiments. This might indicate a different crystal form of canavalin; however, confirmation by x-ray diffraction analysis is needed. After five weeks the pH of all solutions at 10°C in this second batch experiment was measured. Again, we observed an increase from the initial pH in those solutions that contained crystals to as high as 6.94 even though the solutions were buffered at pH=6.5 !

In summary, our studies have corroborated the complexity of earlier, preliminary canavalin solubility findings, which revealed some trends in temperature, pH and salt concentration dependence [4]. Unfortunately, canavalin has proven to be a very difficult protein with which to work. Each batch of canavalin seems to behave differently with respect to the resulting crystal form grown, time required to grow crystals, etc.. Hence, it has been difficult to obtain reproducible results. Also, it appears that the solubility depends much more strongly on pH than on temperature (as observed in general crystallization experiments with the protein and from the solubility studies). We therefore conclude, that canavalin seems to be an inappropriate candidate for crystallization via temperature control.

Scintillation method results on the retrograde solubility of equine serum albumin will be presented in the Final Report for NASA Grant NAG8-824.

3. Thermostated Solution Cell with Growth Sting

3.1 Experimental setup

A small thermostated glass cell with growth sting was designed to utilize the temperature dependence of protein solubility. As depicted in Fig. 16, the flow-through jacket of the cell is formed by an outer wall and a concentric solution chamber. The common bottom is attached to a thermostated (cold) finger or sting. After loading with around 0.7ml of solution, the cell is sealed with silicon high vacuum grease and a cover glass. The interior of the solution chamber and surface of the sting is observed with a long focal length microscope. The temperatures of the jacket and the sting are controlled separately through liquid flows from constant temperature baths. Thus a radial temperature gradient can be established on the sting. and, consequently, the initial nucleation on sufficient supersaturation of the solution can be restricted to the central region of the sting. Appropriate temperature programming

permits one to prevent further nucleation once crystallites have formed, and even to reduce the number of crystallites in order to prevent intergrowth.

3.2 Growth experiments

The growth cell has been tested with lysozyme, canavalin and equine serum albumin. Canavalin was found to be not well suited for temperature control of nucleation and growth, since its temperature dependence of the solubility is not that strong enough; see Section 2.4.2. For ESA it has been difficult to control the nucleation without solubility data, which were not available at that point. We will perform further ESA sting growth experiments whence a solubility diagram is developed (under Grant NAG8-824). With lysozyme we have been able to demonstrate all expected benefits of this growth technique.

The lysozyme solutions used in the growth sting experiments were prepared as outlined in Sect. 2.3.1. In the following we will describe a typical nucleation and growth experiment. A 50 mg/ml lysozyme solution with 2.25% NaCl, 0.05M acetate buffer, pH 4.5, 0.01% NaN₃ was placed into the growth chamber. Note that according to Fig. 11, such a solution composition corresponds to an equilibrium (saturation) temperature of about 30°C. After covering and sealing the cell, T_S and T_J were lowered to about 15°C. Within 12 - 24 hours at this temperature, as shown in Fig. 17, numerous crystals formed in the growth chamber. Then T_S and T_J were slowly ramped to 35°C and 40°C, respectively, which caused most crystals to dissolve except for a few on the central part of the sting; see Fig. 18. T_S and T_J were then decreased to 20°C and 25°C, respectively, where the remaining crystals grew. Lysozyme crystals up to 1.3 mm size were thus grown in the sting cell. Note that in most recent experiments with this arrangement, we have succeeded to nucleate and grow only 1-3 crystals at one time; details will be given in the Final Report for Grant NAG8-824.

The growth rate of two crystals was monitored at 20°C. After 1.2 hours both crystals were growing at a rate of 0.0094 × 0.018 mm/hour. After 5.5 hours the growth rate of both crystals had decreased to 0.0074 × 0.0099 mm/hour. At this time the crystal sizes were 0.149 × 0.128 mm and 0.128 × 0.128 mm.

In addition to demonstrating the feasibility of nucleation and growth control we have obtained interesting qualitative insight from lysozyme experiments in the growth chamber. It was observed that, after repeated nucleation/dissolution during an experiment, "ghosts" of dissolved lysozyme crystals were present on the surface of the sting. These "ghosts" were believed to be denatured protein resulting from the temperature ramping. Furthermore, depending on the degree of supersaturation at which nucleation occurred, the tetragonal crystals that formed and grew had different aspect ratios. Figures 19 and 20 show crystals that nucleated at 10°C and 18°C and grew at 20°C from lysozyme solutions of the same initial concentration, salt, pH, and buffer conditions. Furthermore, we found, as expected, that fewer

crystallites formed if nucleation was induced at lower supersaturation. Though these considerations are commonplace in inorganic crystallization, it is comforting to see the same physiochemical principles underlying protein crystal growth.

4. Microscopic Growth Kinetics Studies

4.1 *Microscopic growth cell*

After the construction and testing of a prototype microscopically accessible growth cell for kinetics studies (described in earlier progress reports), it became clear that a novel design was required to fully utilize the high resolution provided by state-of-the-art microscopy. The preliminary microscopy studies showed that reflection microscopy will not reveal feature sizes of the small dimensions desirable for definitive kinetics studies, probably due to a too small difference in refractive index between lysozyme crystals and solutions. Hence, we purchased from Alabama State funds a Leitz illumination condenser with Wollaston prism and lenses for transmission interference microscopy. This technique, however, requires the positioning of the (crystal-solution) interface to be observed to within 2 mm of the edge of the condenser head. With the prototype design this distance could not be made shorter than about 30mm.

Figure 21 presents a cross-sectional drawing of the novel microscopic growth cell developed in our group. A liquid bridge of 25 μ l of protein solution is suspended between two 0.19mm thick cover glasses which are held about 1.0mm apart by a brass cell holder. Attached to the cell holder are 4 thermoelectric (Peltier) heat pumps connected in series to a Marlow model 5010 temperature controller/power supply. A bead thermistor placed in a bore of the cell holder monitors the temperature. The outer sides of the Peltier units are in contact with a water cooled tilt ring that acts, respectively, as heat sink or source in the cell cooling or heating mode. With this arrangement, the temperature of the cell holder can be programmed between 4°C and 50°C with a stability of $\pm 0.1^\circ\text{C}$.

Note that besides providing a reasonably stable heat sink/source, the water cooled tilt ring is suspended via a gimbal arrangement within the turntable ring. The tilt axis can be chosen by rotating the ball spacer ring. This, in turn, repositions the two oppositely placed ball bearings that are precisely fitted into the grooves of the turntable and the tilt ring. Consequently, the cell holder can be rotated or tilted until a crystal face of interest is aligned normal with respect to the optical axis of the microscope. These features are critical in finding the crystal positioning which is necessary to produce interference fringes on a given crystal surface.

4.2 Image storage and processing system

During an in-situ growth kinetics study, there are numerous morphological features (growth steps, spatially varying shifts of interference fringes, etc.) to be observed simultaneously. The rate with which such features change significantly often exceeds the frequency with which films can be replaced, say, in a Polaroid film holder. In addition, during interferometric observations (with the microscope on a vibration isolation table) such film changes, or camera motor-induced vibrations would jeopardize the image quality. Hence, it was decided to design and acquire a magnetic image storage system with continuous recording capability, combined with an image processing system that allows for post-experiment image enhancement required for full resolution utilization of the interferometric studies. In preliminary tests it became clear that the limited resolution of about 400x400 pixels of commercial systems available at the beginning of this grant would be insufficient to store images with a resolution comparable to that of our Leitz research microscope. Therefore we have designed, with help from the TECON corporation, a new system from components with 1024x1024 lines of resolution. This image storage and processing system consists of:

- Dage MTI Precision 81 high resolution TV camera with Pasecon video tube
- Dage HR-2000 monitor
- Grundig BK224 high resolution video recorder
- Compaq Deskpro 286 personal computer with 640k RAM, 40 Mb hard drive, two 1.2 Mb 5 1/4" floppy drives, Compaq VGA high resolution monitor and high resolution Logitech mouse
- Univision UDC 2600-12M display board
- TECON DVX 1024 frame grabber
- Image-Pro II software (IP2UDC)
- Customized software for freeze frame video to capture high resolution 1024² images.

Figure 22 shows a flow chart of the image storage and processing system. In short, the system allows for real time video recording of the microscopic images that can be recalled in their analog form for the identification of crucial events and for rate determinations of feature changes. Select images are then saved in digital form in the host computer for image analysis and processing. Features of the Image-Pro software enable us to perform, among other things, pixel-by-pixel intensity histogram analyses (256 grey scales), line distance and angle measurements, spatial frequency filtering as well as contrast changes through stretching and sliding of intensity distributions.

The power of this system became apparent, for instance, when features which are barely discernable through the microscope eye pieces, become clearly visible when 'seen' through the eye of the camera, even without significant image enhancement, often only through contrast changes on the TV monitor. These features can, of course, be further enhanced as indicated above.

In addition to the features of this system, newly acquired interferogram analysis software (NASA Grant NAG8-790) is available for the analysis of interferograms. The ZAPP-PC software digitizes the fringe pattern and performs analyses of interferograms, including fitting to Zernike polynomials and removal of aberrations from the data. This advanced graphics capability allows interactive screen displays of 3-D phase plots, x-, y-, and radial profiles, and contour plots.

4.3 Preliminary results

Utilizing the lysozyme solubility information gained with the scintillation cell (Sect. 2.3.2), we have begun to investigate the growth and dissolution of lysozyme crystals in the microscopic growth cell. The solutions studied thus far have all contained about 50 mg/ml lysozyme, 2.5% NaCl and have been buffered to a pH of 4.5 via a 0.05 M sodium acetate buffer; for preparation see Sect. 2.3.1. In several experiments we have been able to obtain only one or two faceted lysozyme crystals at one time in the growth cell. The temperatures and induction times for the nucleation of these crystals have been reproducible. Also, the solubility curves were found quite reliable for the prediction of the temperatures at which growth and dissolution will proceed on existing crystals. For example, a lysozyme crystal that in agreement with Fig. 11 showed hardly any feature changes at 32°C, began clearly to etch at 33°C and to regrow at 31°C. This nicely corroborates the solubility data obtained with the scintillation technique.

We found that growth temperature changes of 2°C lead to pronounced ghost images (outlines of the crystal surface prior to the temperature change) in the crystal. But our most recent experiments seem to indicate that even significantly smaller temperature changes can cause some "veiling" of lysozyme crystals. Such ghosts and veils, in analogy to observations from inorganic solution crystal growth, possibly indicate some irregular incorporation of solution. It should be noted that the finer veils cannot be detected with reflected light microscopy and are only discernable in the differential interference transmission mode with very careful focusing and viewing with the high resolution camera and monitor. Thus, we suspect that such fine veiling remained unnoticed in most protein crystal growth experiments to-date. The consequences for x-ray diffraction resolution of veiling, which will certainly lead to a reduction of the lattice regularity, remains to be investigated.

5. Growth Experiments in Thermosyphon Flow

Pusey et al. [9] showed that forced convective flow over tetragonal lysozyme single crystals caused a reduction in growth rate. These experiments were conducted with crystals mounted on walls of flow-through chambers. We wanted to investigate the interaction of flow with growth behavior in a configuration in which the crystal is more freely exposed to the flow, than in the vicinity of a wall in which the flow is difficult to quantify on the small scale involved. Consequently, under a small NASA Grant (NAS8-098) we began growth experiments with lysozyme in which the crystals were freely suspended in a flow. These experiments were completed under this grant and are summarized in the following two Sections.

5.1 *Thermosyphon technique*

A schematic of the thermosyphon loop is shown in Fig. 23. A cooling jacket keeps the right side of the loop at some lower temperature while the left side is heated. Solution circulation is induced by bouancy that results from the density difference in this temperature differential. The lower part of the loop is insulated so that the solution temperature at the location of the suspended crystal is essentially the same as that at the bottom of the cooled section. The temperature difference is chosen such that (i) the flow velocity is high enough to compensate for the settling velocity of the crystal, which remains freely suspended and (ii) sufficient supersaturation is obtained at the suspended crystal to drive its growth. Note that the lower bend and the section entering the expansion chamber are made of smaller cross section tubing. This causes a locally higher velocity to aid the suspension of crystals in the expansion chamber. For details of the heat transfer to the solution, calculation of resulting velocities and suspension forces, as well as the procedures leading to in-situ nucleation and growth see [10,11, see attachments].

5.2 *Results with lysozyme*

A series of experiments were aimed at growing **tetragonal** lysozyme in the thermosyphon flow. Nucleation occurred as expected and crystallites were trapped in the expansion chamber [10]. Surprisingly, though, the crystal sizes did not exceed 0.1mm irrespective of suspension time in the supersaturated solution, even under supersaturation conditions high enough to cause continuous nucleation. Microscopic examination revealed that the crystals lacked well defined facets. Also, seeds of 0.1mm and larger sizes, introduced through the upper port showed no growth. However, tetragonal lysozyme crystals that had reached their terminal size in the thermosyphon showed uninhibited growth upon transfer to stagnant control solutions.

Similar experiments were performed under conditions favorable for the growth of **orthorhombic** lysozyme; see Sect. 2.3.2. In contrast to the results obtained with the

tetragonal form there was no cessation of growth and crystals (nucleated in-situ as well as seeded) grew to their suspension limit.

At this point there is no clear explanation of these observations. The cessation of growth of the tetragonal form may be either due to some mechanical aspects of the suspending shear flow, although recent model calculations by Grant and Saville [12] suggest that the torques exerted by such flows on protein molecules on the crystal surface are small as compared to bond strength. On the other hand, due to the thermal cycling of the solution in the thermosyphon, there may be some kinetic reasons for the cessation [10].

In addition to these important results, these experiments also gave some insight essential for the development of successful seeding techniques. We found, for instance, that if a tetragonal lysozyme seed experiences a temperature change of several degrees during transfer to a supersaturated solution, it will not grow thereafter. Furthermore, when the solution a seed was transferred to differed in salt concentration by 0.003 gm/ml, no growth occurred. Hence, before seed transfer, special measures had to be taken to assure equilibration of the seed to the salt concentration of the solution to be seeded [10].

6. Mathematical Model for Concentration Distribution in Hanging Drop at Low Gravity

To estimate the concentration gradients that may arise in the vapor diffusion technique at the surface of hanging drops in the absence of convective flows, we have performed model calculations lysozyme-NaCl and myosin-NaCl solutions [13, see attachments]. To make the model as realistic as possible, the influence of the salt concentration on water vapor pressure and, thus, on evaporation was taken into account. Also, vapor diffusion across an air gap was included. Dimensions were chosen that are typical of protein growth practice. We found, as illustrated by Fig. 24, that in the case of myosin, due to its low diffusivity, significant gradients can arise in the drop. The steepening concentration (density) profiles depicted in Fig. 24 may have significant implications for the possible development of convective instabilities in the drop at low, but finite, gravity levels.

7. Summary

In this work we have shown that the temperature dependence of protein solubilities can expediently and accurately be determined with a scintillation (light scattering) technique. Solubility data can be advantageously used for the control of nucleation and growth of protein crystals through temperature. Forced convective flows can be detrimental to protein crystal growth. Under purely diffusive transport conditions, severe protein concentration gradients can develop in the hanging drop evaporation technique.

8. References

- [1] F. Rosenberger, Inorganic and protein crystal growth - similarities and differences, *J. Crystal Growth* 76 (1986) 618.
- [2] F. Rosenberger and E.J. Meehan, Control of nucleation growth in protein crystal growth, *J. Crystal Growth* 90 (1988) 74.
- [3] S.B. Howard, P.J. Twig, J.K. Baird and E.J. Meehan, The solubility of hen egg-white lysozyme, *J. Crystal Growth* 9 (1988) 94.
- [4] R.C. DeMattei and R.S. Feigelson, The Solubility Dependence of Canavalin on pH and Temperature, Final Technical Report on Protein Crystal Growth in Low Gravity, NASA NAG8-489, CMR-88-9, Stanford SPO#1018, Period January 1, 1987 through June 30, 1988 (1988).
- [5] M. Pusey and K. Gernert, A method for rapid liquid-solid phase solubility measurements using the protein lysozyme, *J. Crystal Growth* 88 (1988) 419.
- [6] Marc Pusey, Personal communication, Marshall Space Flight Center, Space Sciences Laboratory, Huntsville, Alabama.
- [7] S.C. Smith, S. Johnson, J. Andrews and A. McPherson, Biochemical characterization of canavalin, the major storage protein of jack bean, *Plant Physiology* 70 (1982) 1199.
- [8] A. McPherson and R. Spencer, Preliminary structure analysis of canavalin from jack bean, *Arch. Biochem. Biophys.* 169 (1975) 650.
- [9] M. Pusey, W. Witherow and R. Naumann, Preliminary investigations into solutal flow about growing tetragonal lysozyme crystals, *J. Crystal Growth* 90 (1988) 105.
- [10] T. A. Nyce and F. Rosenberger, Growth of Protein Crystals Suspended in a Closed Loop Thermosyphon, *J. Crystal Growth* (in print). **See attachments.**
- [11] T. A. Nyce and F. Rosenberger, General Method for Calculating Velocities and Heat Transfer in Closed Loop Natural Convection Systems, submitted to *International Journal of Heat and Mass Transfer*. **See attachments.**
- [12] M. L. Grant and D. A. Saville, The Role of Transport Phenomena in Protein Crystal Growth, *J. Crystal Growth*, in print.
- [13] J.D. Fehribach and F. Rosenberger, Analysis of models for two solution crystal growth problems, *J. Crystal Growth* 94 (1989) 6. **See attachments.**

9. Figure Captions and Figures

- Figure 1. Schematic of system for temperature controlled protein crystallization and dissolution with detection of crystallites by optical scintillation.
- Figure 2. Lysozyme dissolution with increasing temperature monitored by scintillation signal. Lysozyme concentration 14 mg/ml, 2.5% NaCl , pH=4.5.
- Figure 3. Lysozyme dissolution with increasing temperature monitored by scintillation signal. Lysozyme concentration 48.1 mg/ml, 2.1% NaCl , pH=4.5.
- Figure 4. Lysozyme dissolution with increasing temperature monitored by scintillation signal. Lysozyme concentration 12 mg/ml, 2.5% NaCl , pH=4.5.
- Figure 5. Comparison of lysozyme solubility data obtained with scintillation method (this work) and packed microcolumn method ([6], for method see [5]).
- Figure 6. Comparison of lysozyme solubility data obtained with scintillation and batch methods (this work).
- Figure 7. Solubility versus salt concentration for tetragonal and orthorhombic lysozyme, obtained with batch method at 26°C.
- Figure 8. Solubility versus salt concentration for tetragonal and orthorhombic lysozyme, obtained with batch method at 28°C.
- Figure 9. Solubility versus salt concentration for tetragonal and orthorhombic lysozyme, obtained with batch method at 30°C.
- Figure 10. Solubility versus temperature for tetragonal and orthorhombic lysozyme obtained with the batch method. Note the lower solubility of the orthorhombic form at both salt concentrations.
- Figure 11. Solubility of tetragonal lysozyme versus temperature, scintillation method.

- Figure 12. Canavalin dissolution with increasing temperature monitored by scintillation signal. Canavalin concentration 8.67 mg/ml, 0.77% NaCl, pH=7.2.
- Figure 13. Canavalin solubility versus temperature at various salt concentrations; batch method.
- Figure 14. Canavalin solubility versus salt concentration at various temperatures; batch method. Values indicate final pH; initial pH 5.5 - 6.0.
- Figure 15. Canavalin solubility versus salt concentration at 10°C, batch method. Values indicate final pH; initial pH 6.5.
- Figure 16. Schematic of thermostated cell with growth sting.
- Figure 17. View of bottom of growth chamber of the thermostated cell. Lysozyme crystallites nucleated over entire surface of the growth cell from a 50 mg/ml solution. Nucleation and growth at 15°C. The inner circle outlines the boundary of the cold sting.
- Figure 18. Crystallites of Fig. 17 reduced by dissolution at sting temperature 35°C and jacket temperature 40°C. For details see text.
- Figure 19. Tetragonal lysozyme crystals, nucleated at 10°C, growth at 20°C.
- Figure 20. Tetragonal lysozyme crystals, nucleated at 18°C, growth at 20°C.
- Figure 21. Temperature controlled crystallization cell for in-situ microscopy with reflected and transmitted light.
- Figure 22. Flowchart of image processing system.
- Figure 23. Thermosyphon crystal growth apparatus.
- Figure 24. Calculated concentration profiles for lysozyme and myosin in hanging drop at three times after beginning of water evaporation; for details see [13].

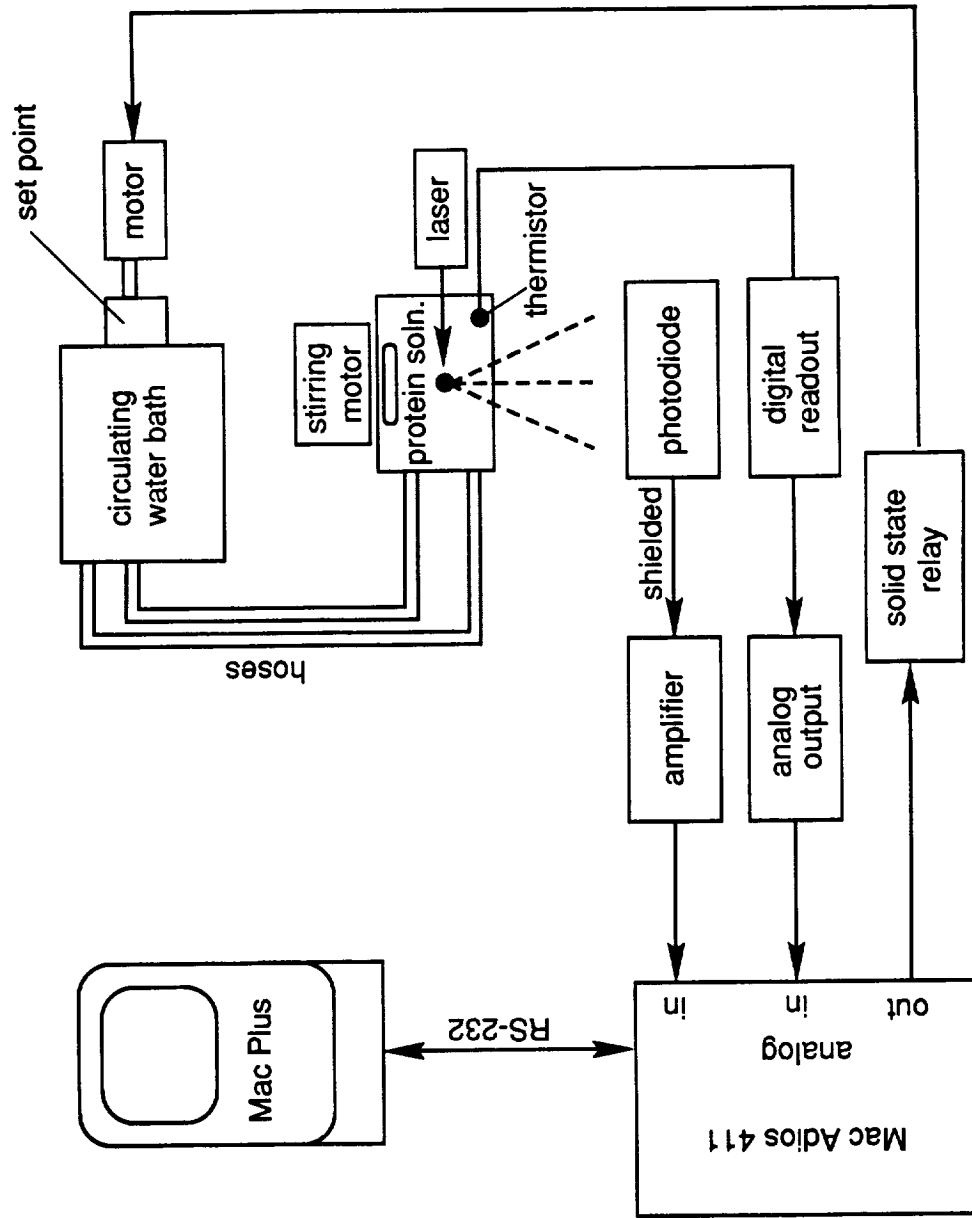


FIG. 1

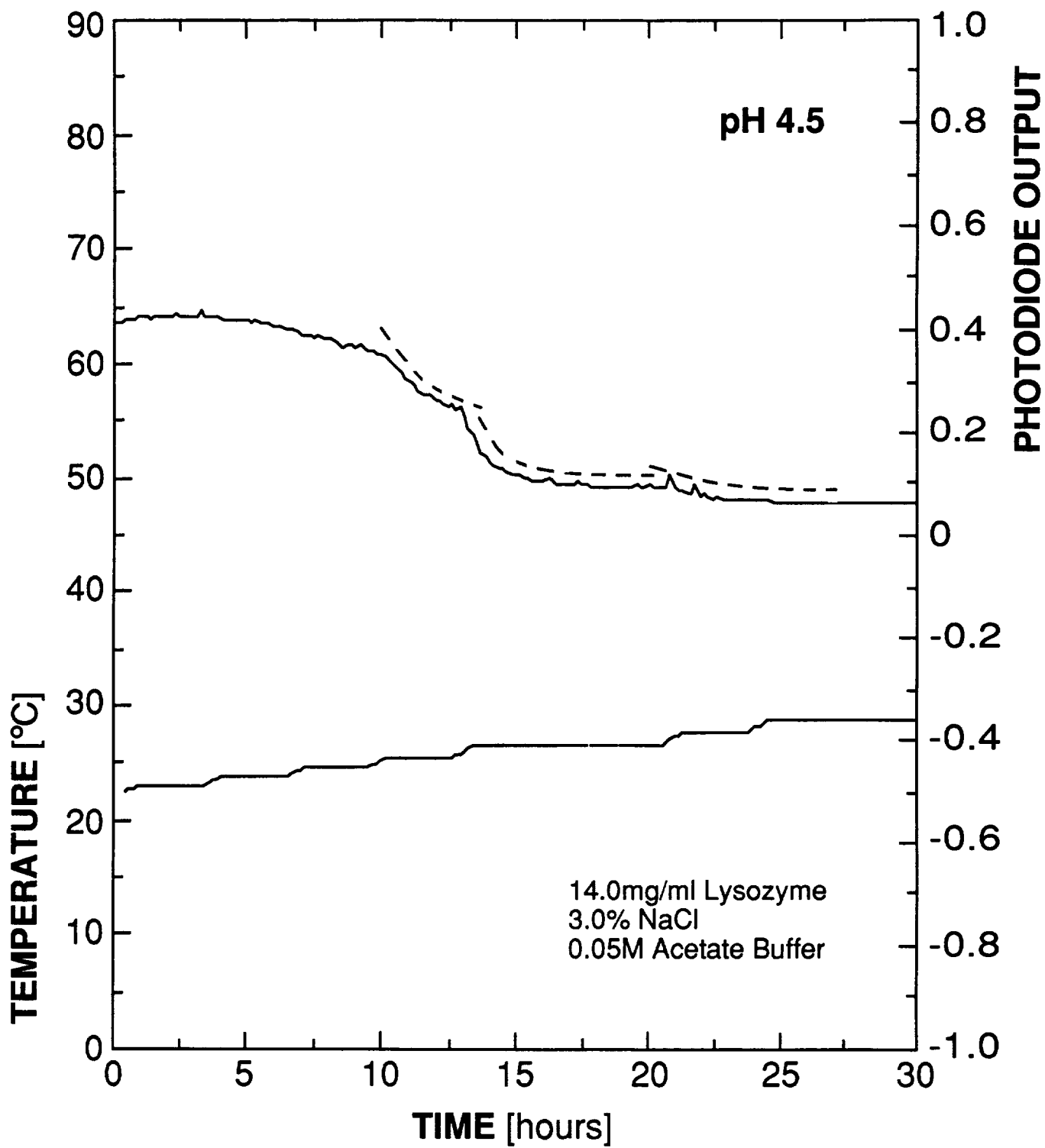


FIG. 2

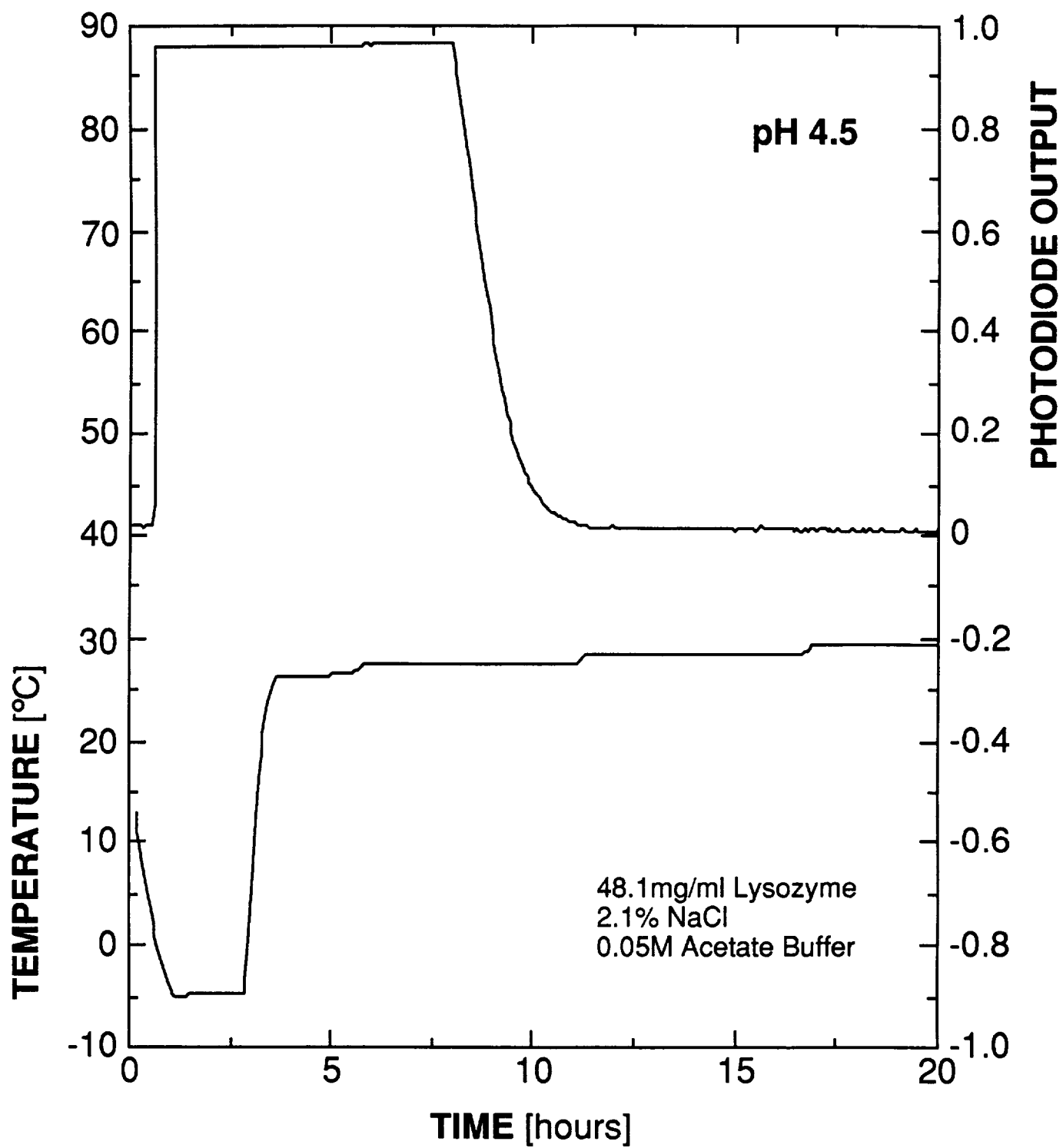


FIG. 3

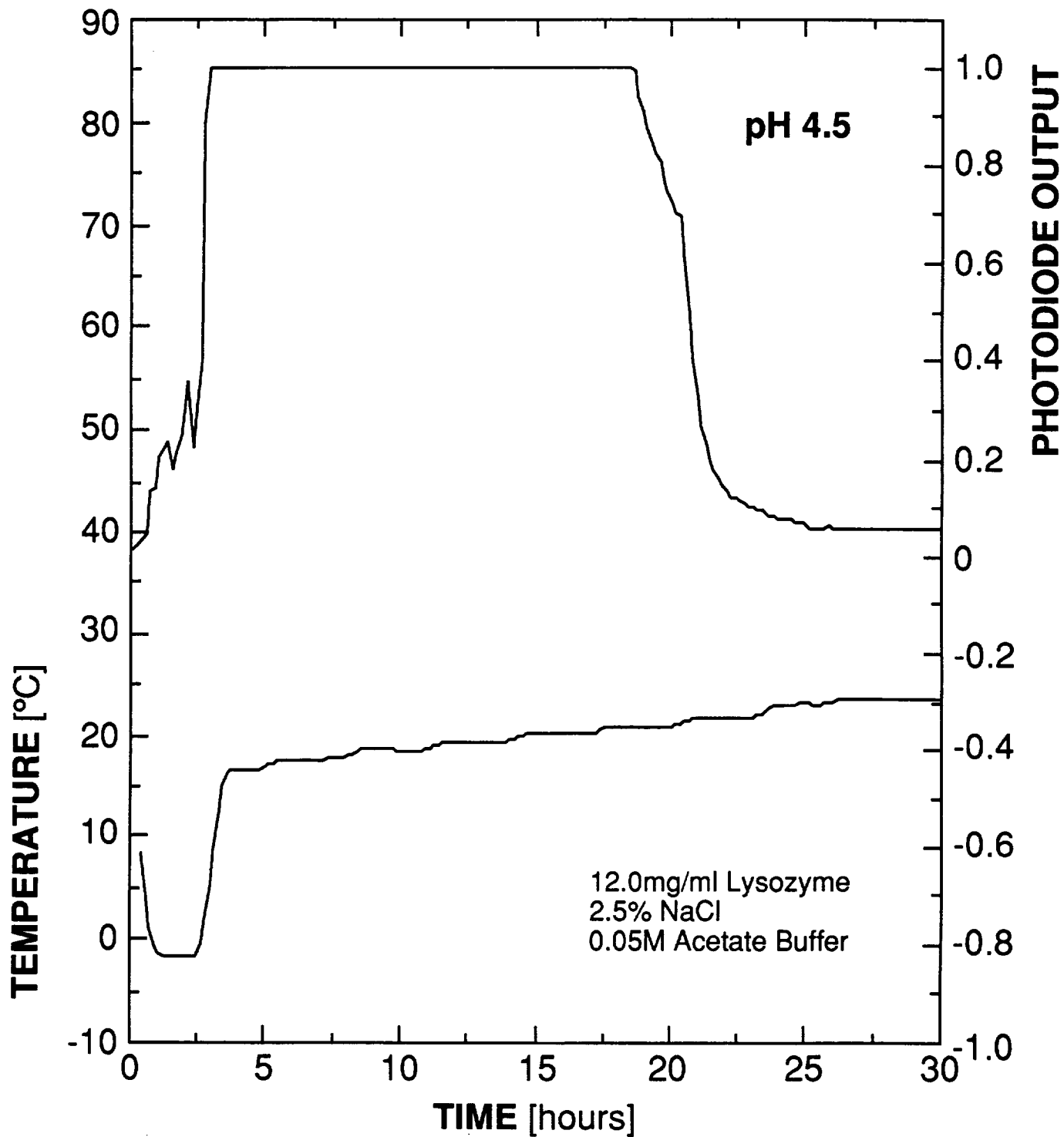


FIG. 4

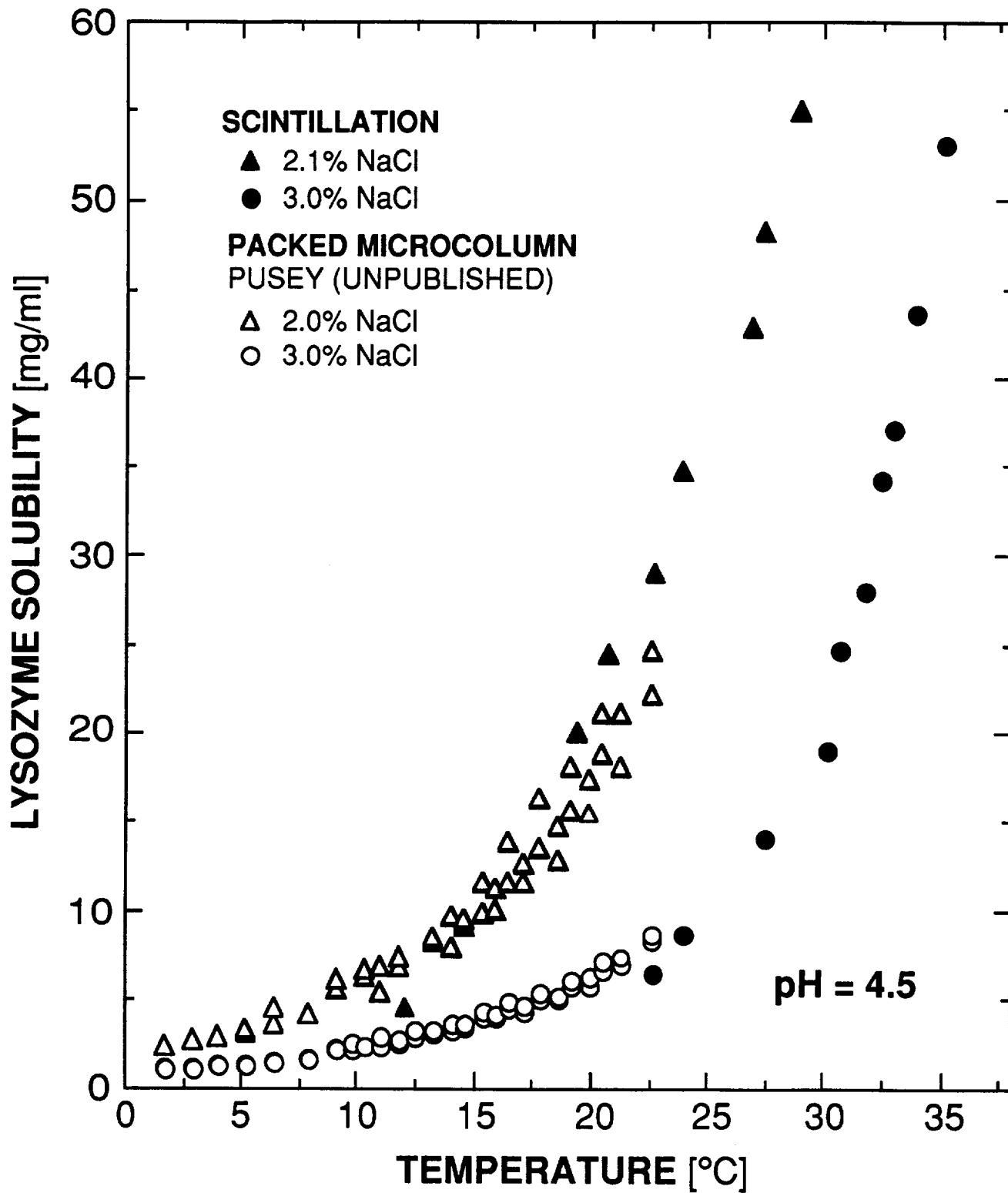


FIG. 5

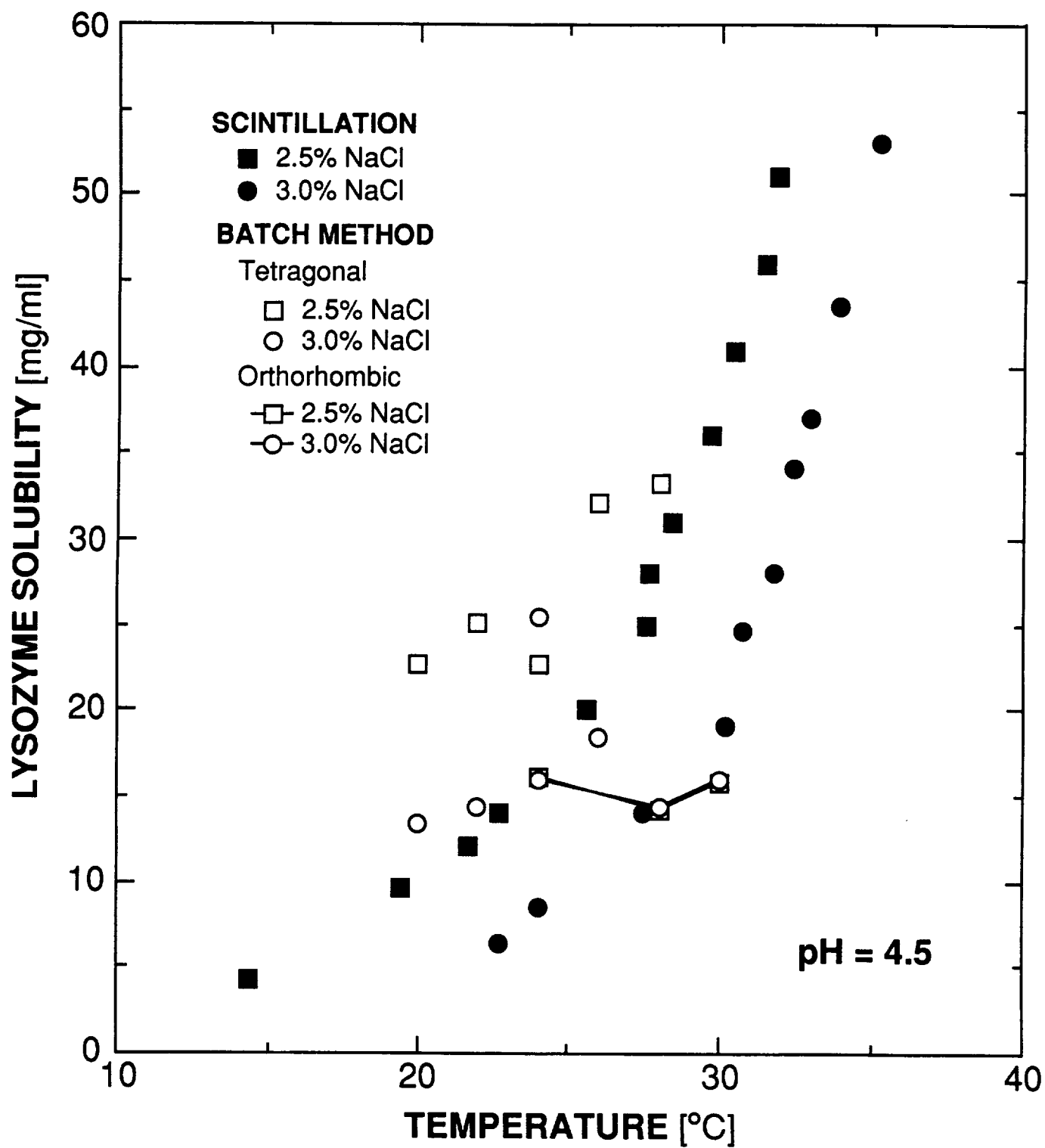


FIG. 6

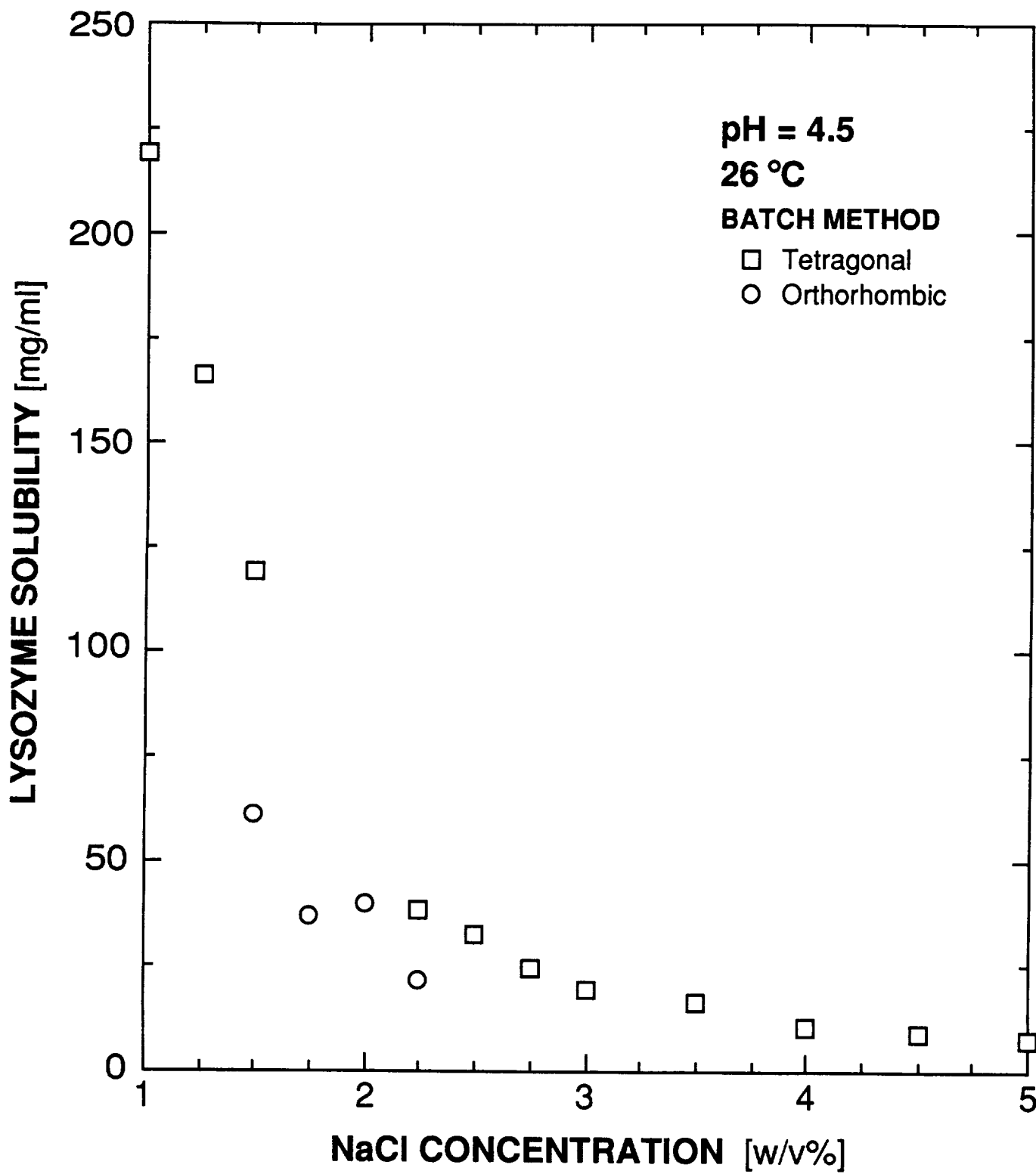


FIG. 7

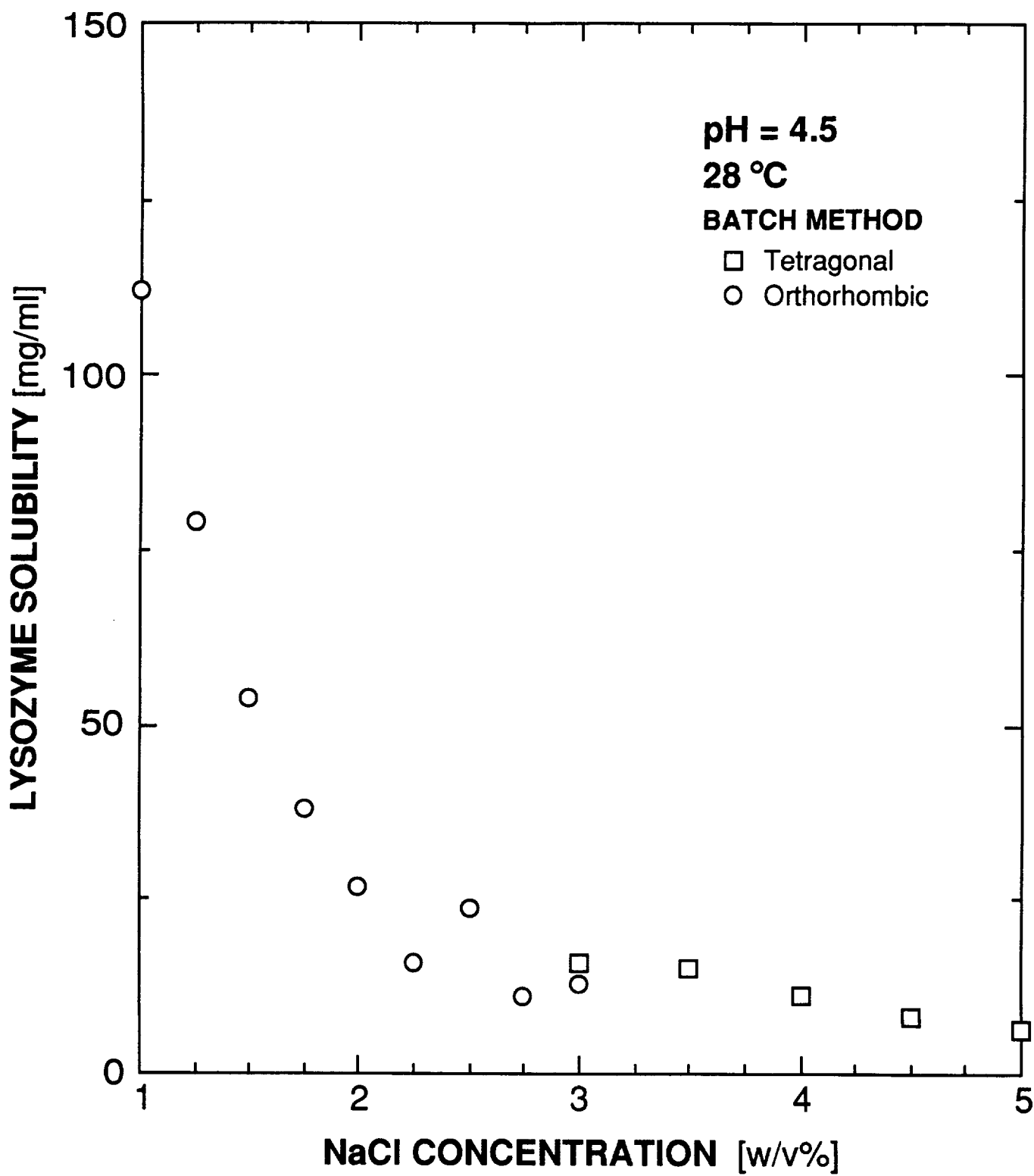


FIG. 8

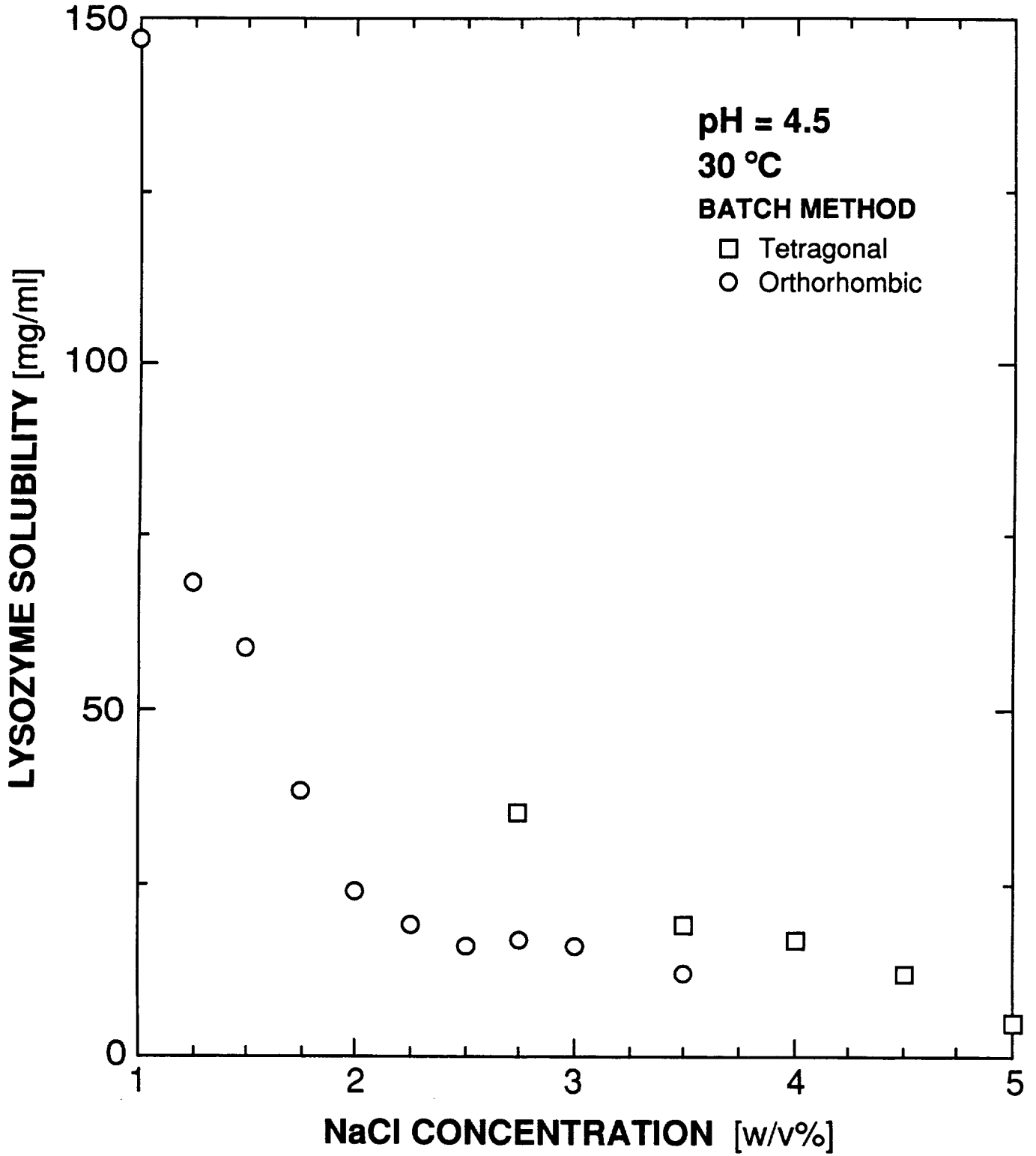


FIG. 9

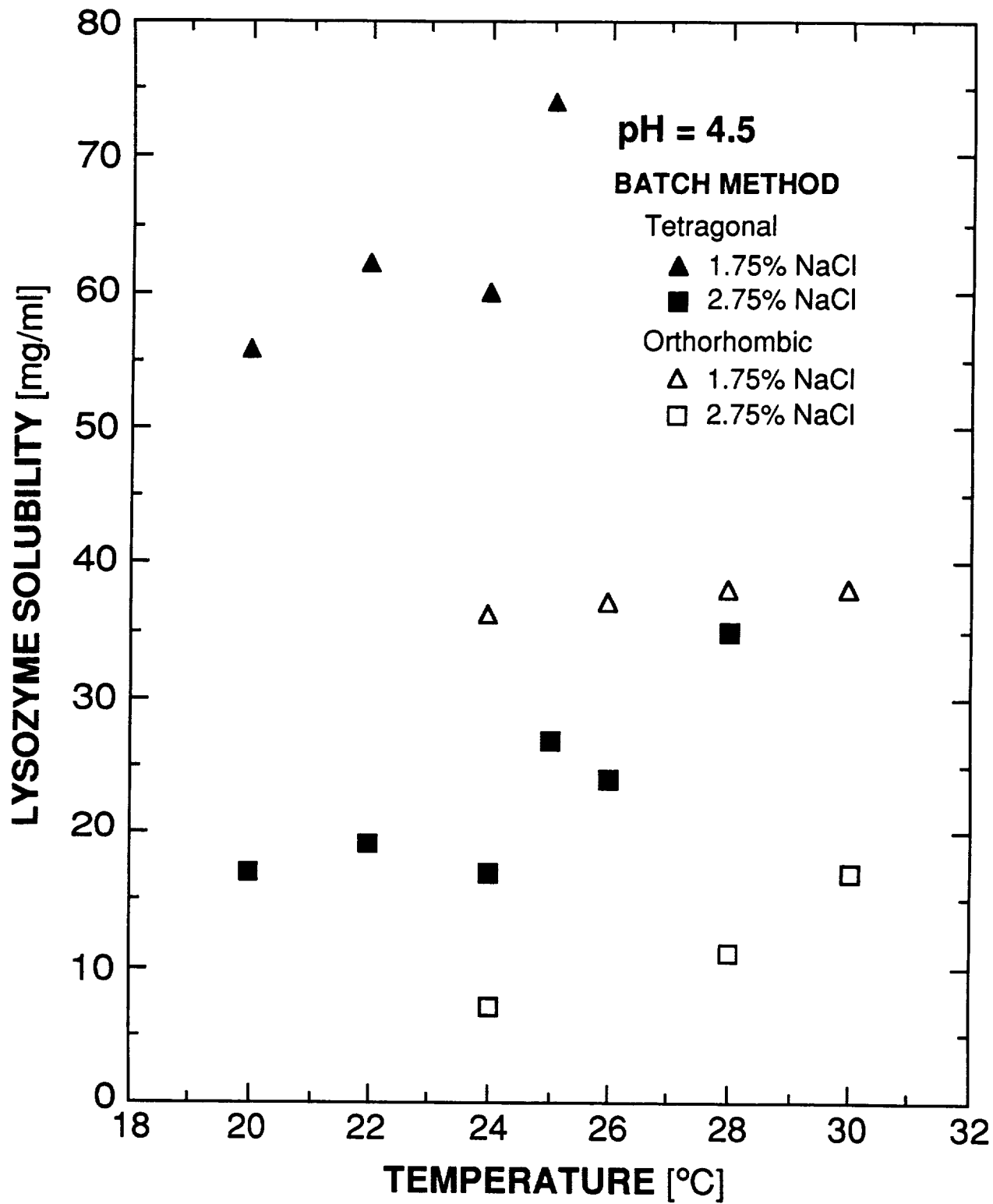


FIG. 10

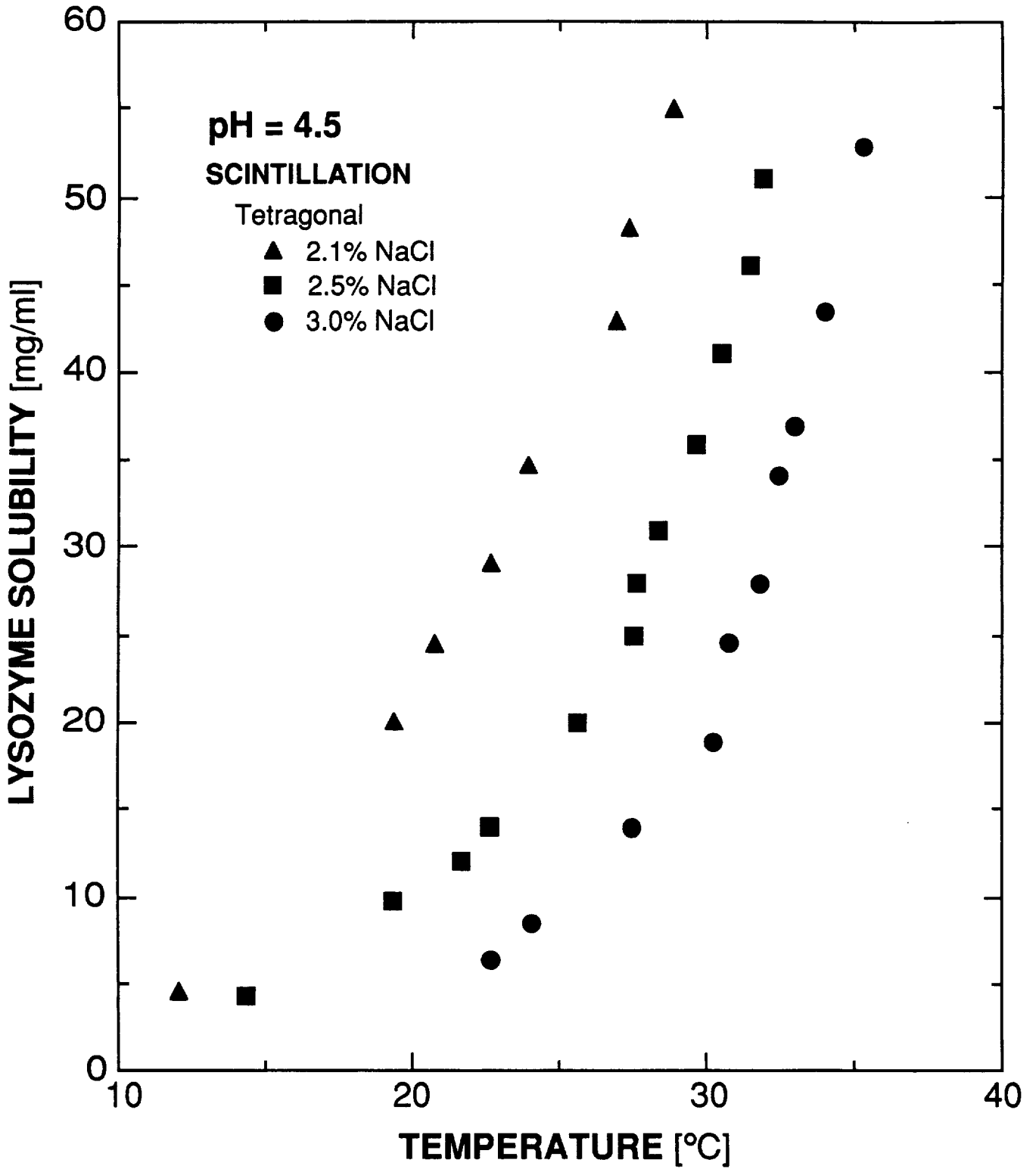


FIG. 11

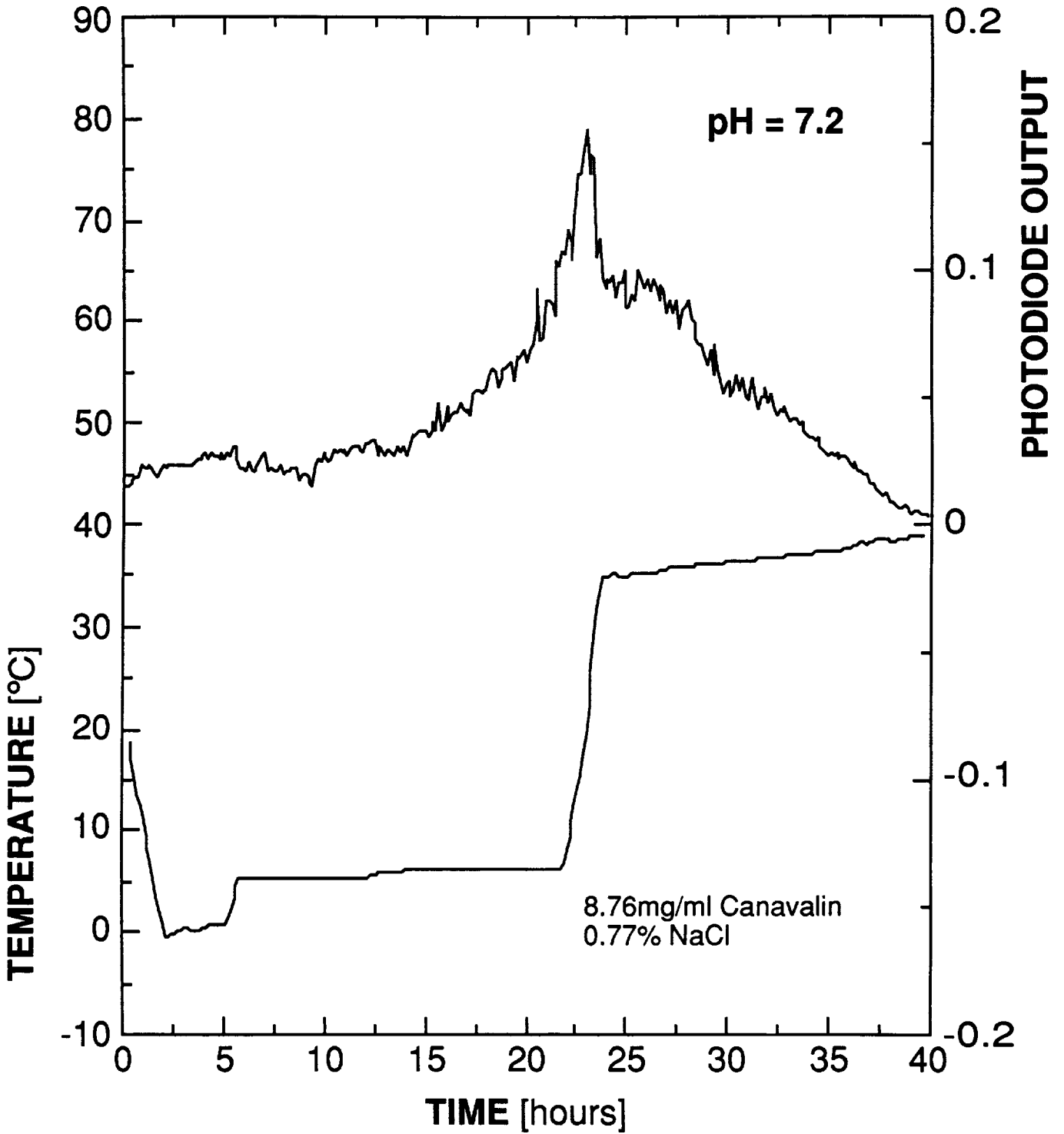


FIG. 12

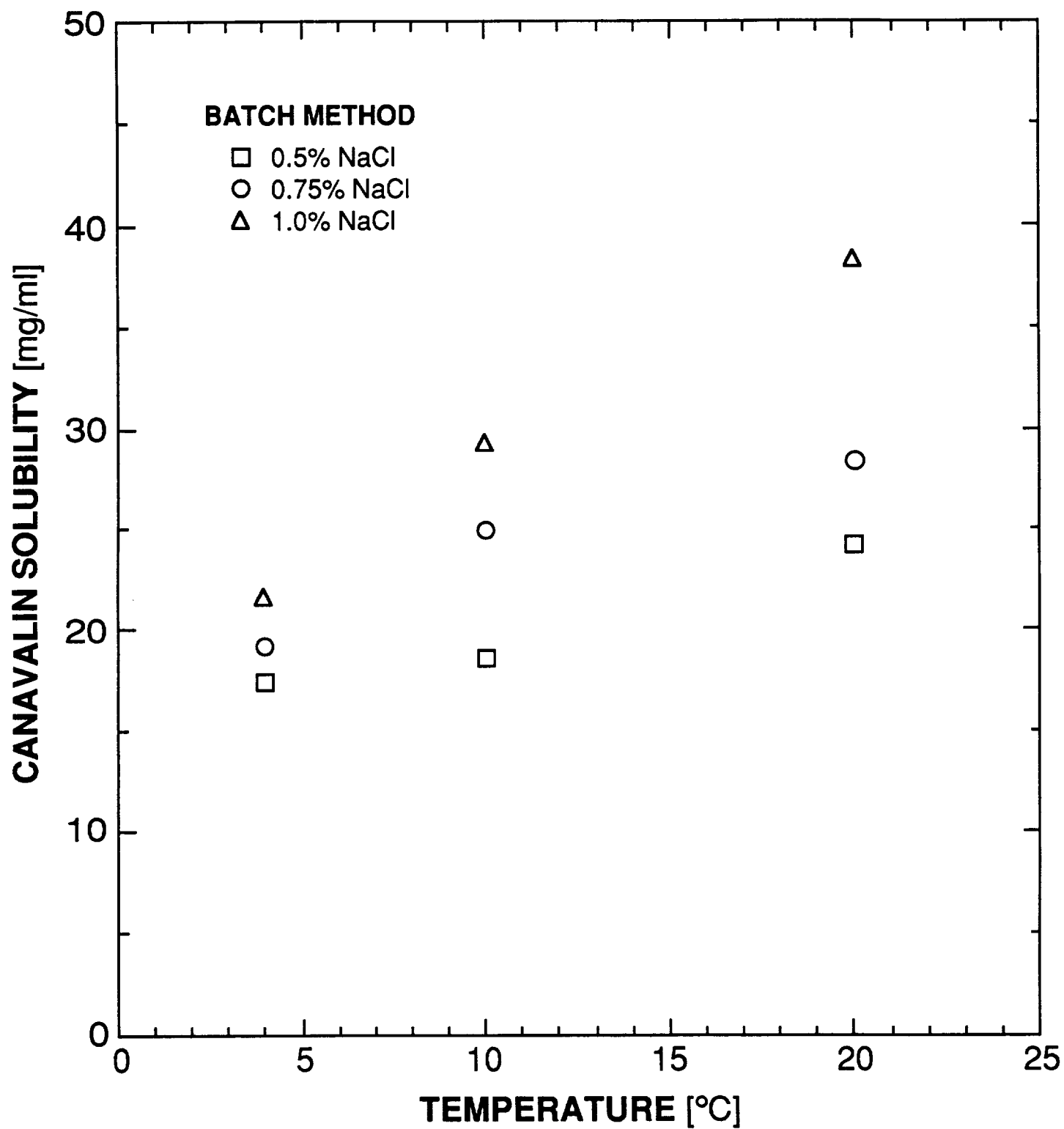


FIG. 13

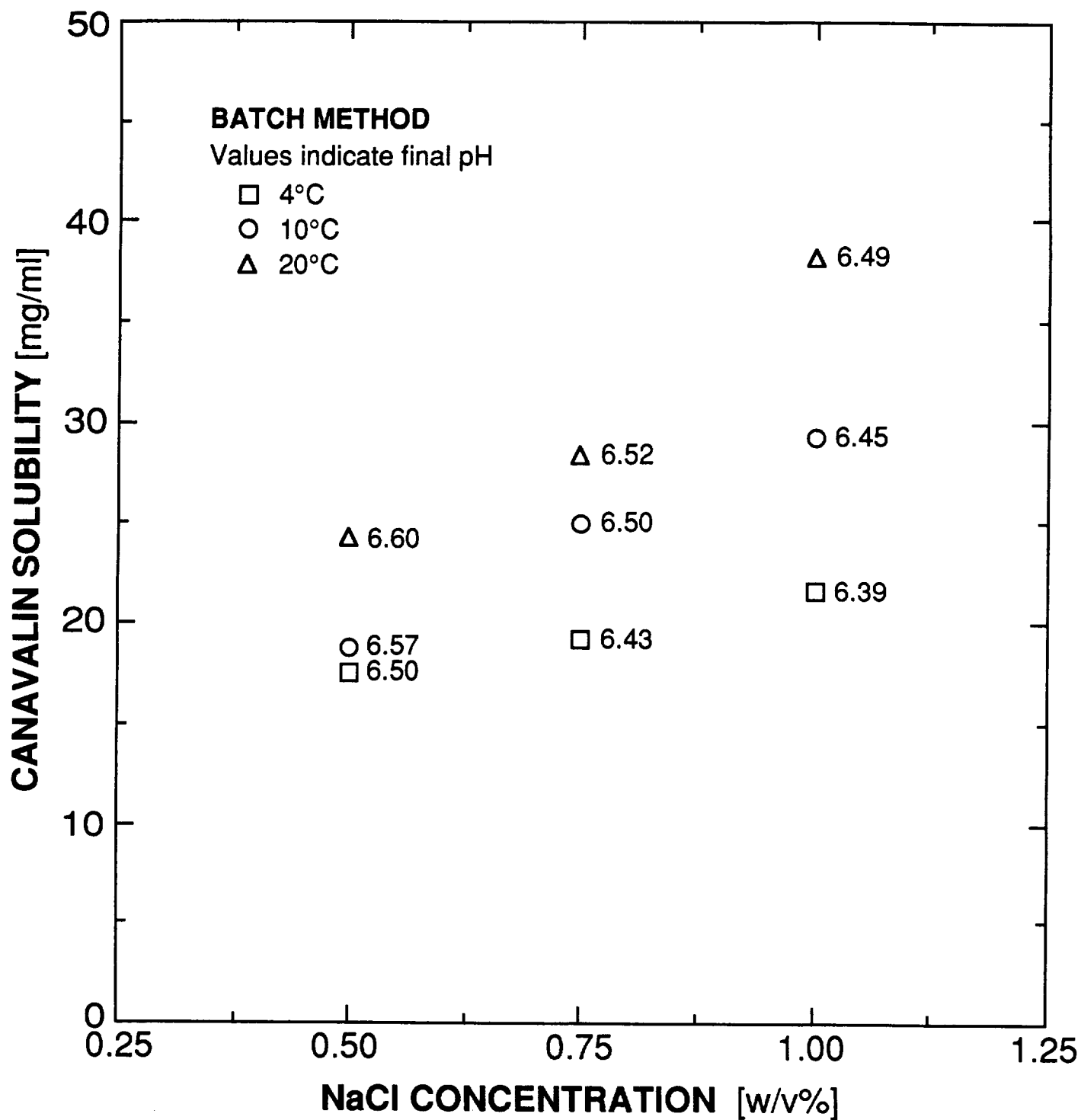


FIG. 14

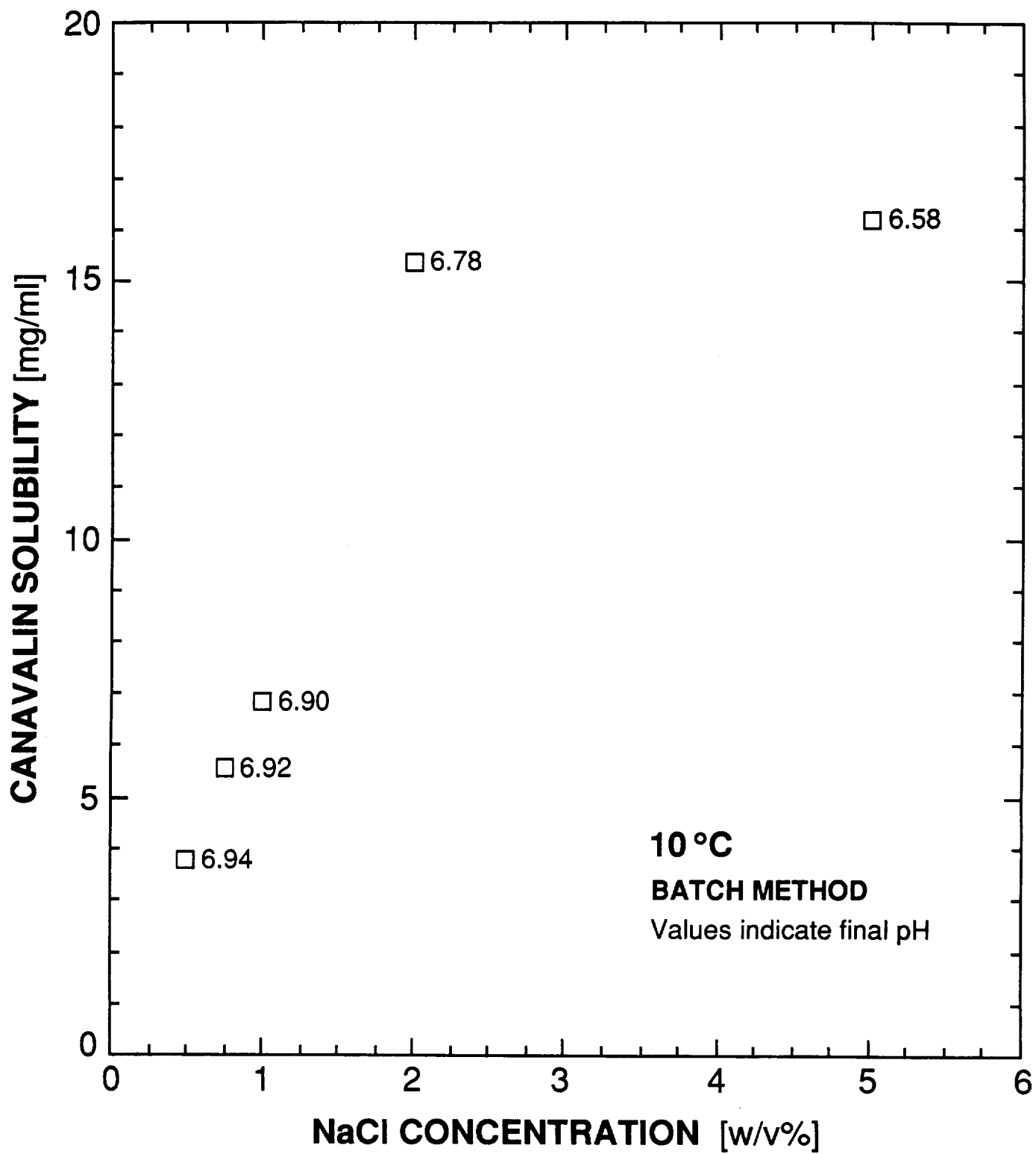


FIG. 15

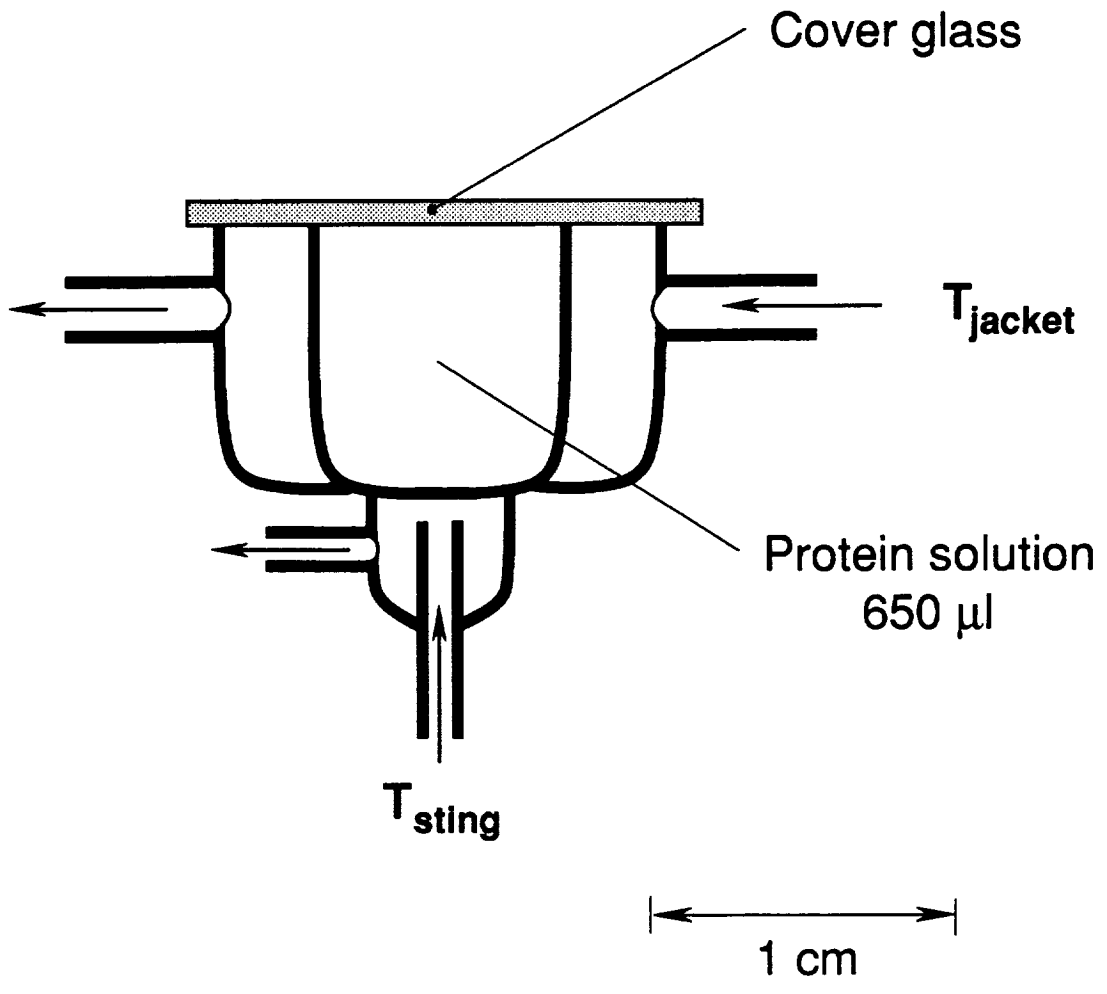
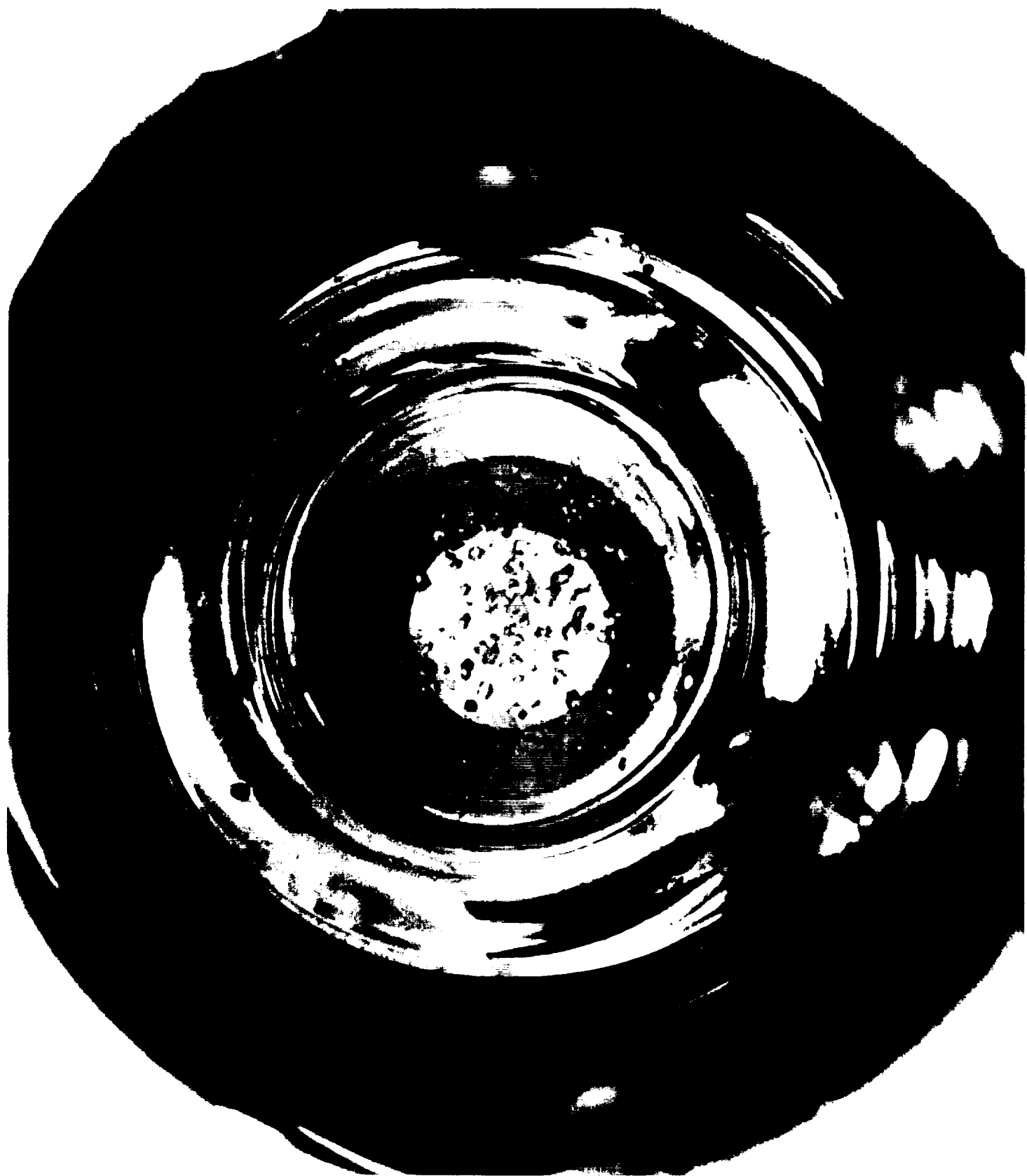


FIG. 16



1 mm

FIG. 17



1 mm

FIG. 18



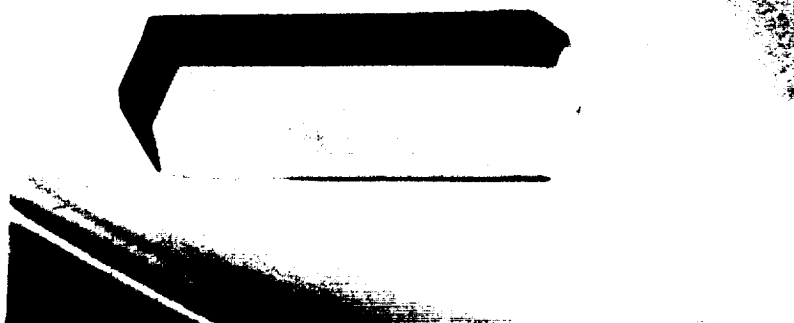
0.2 mm

FIG. 19

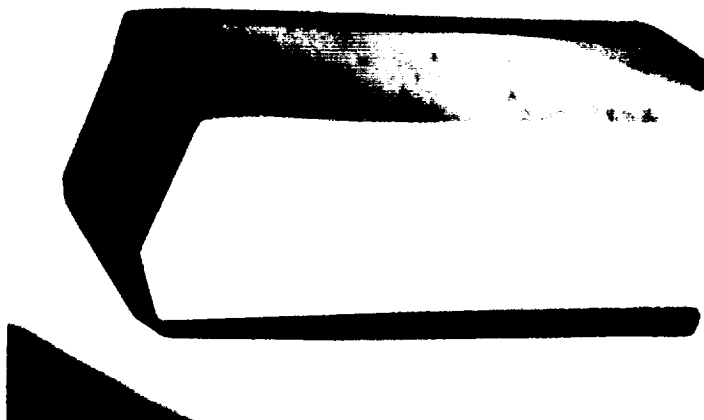
4 days



11 days



16 days



0.2 mm

FIG. 20

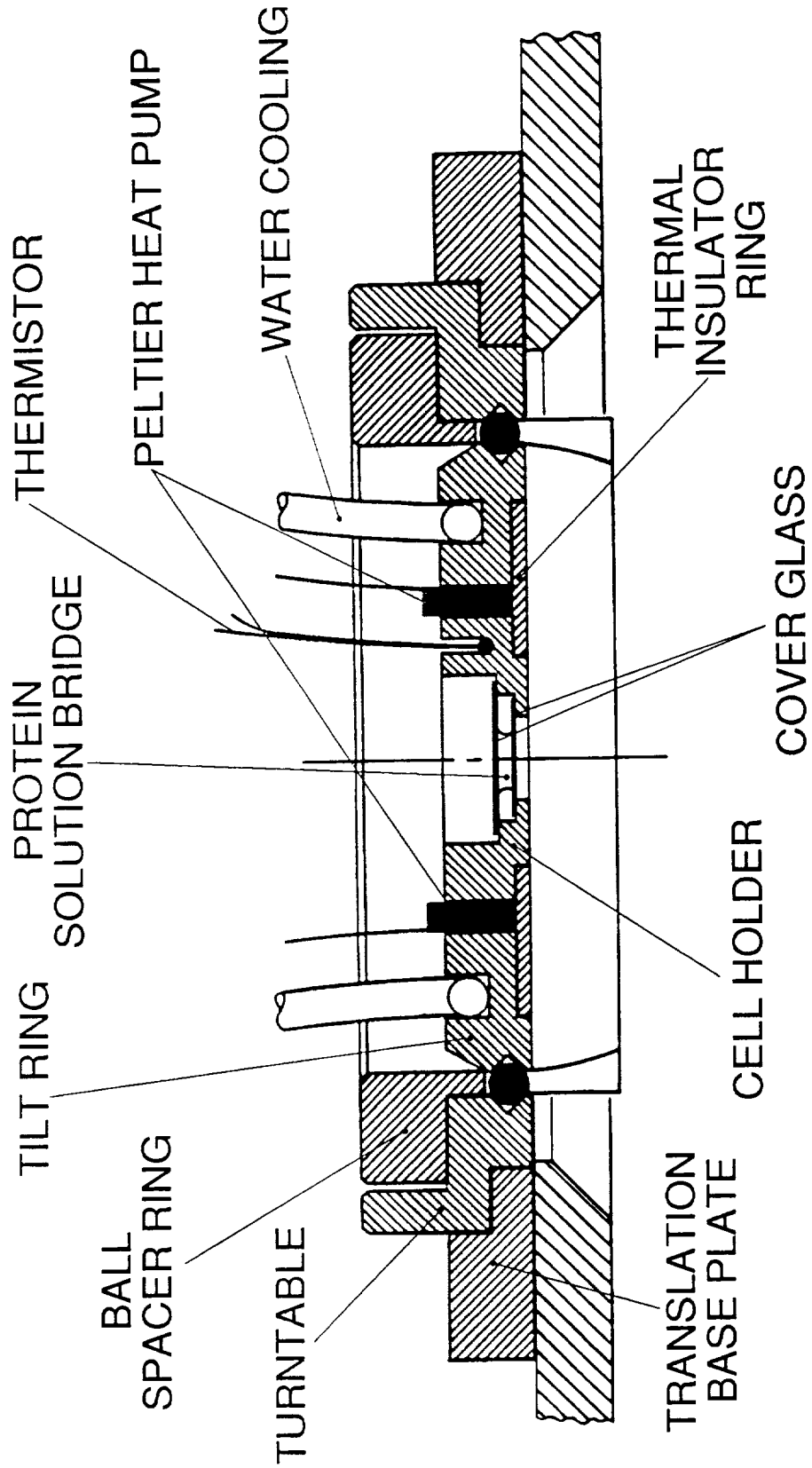


FIG. 21

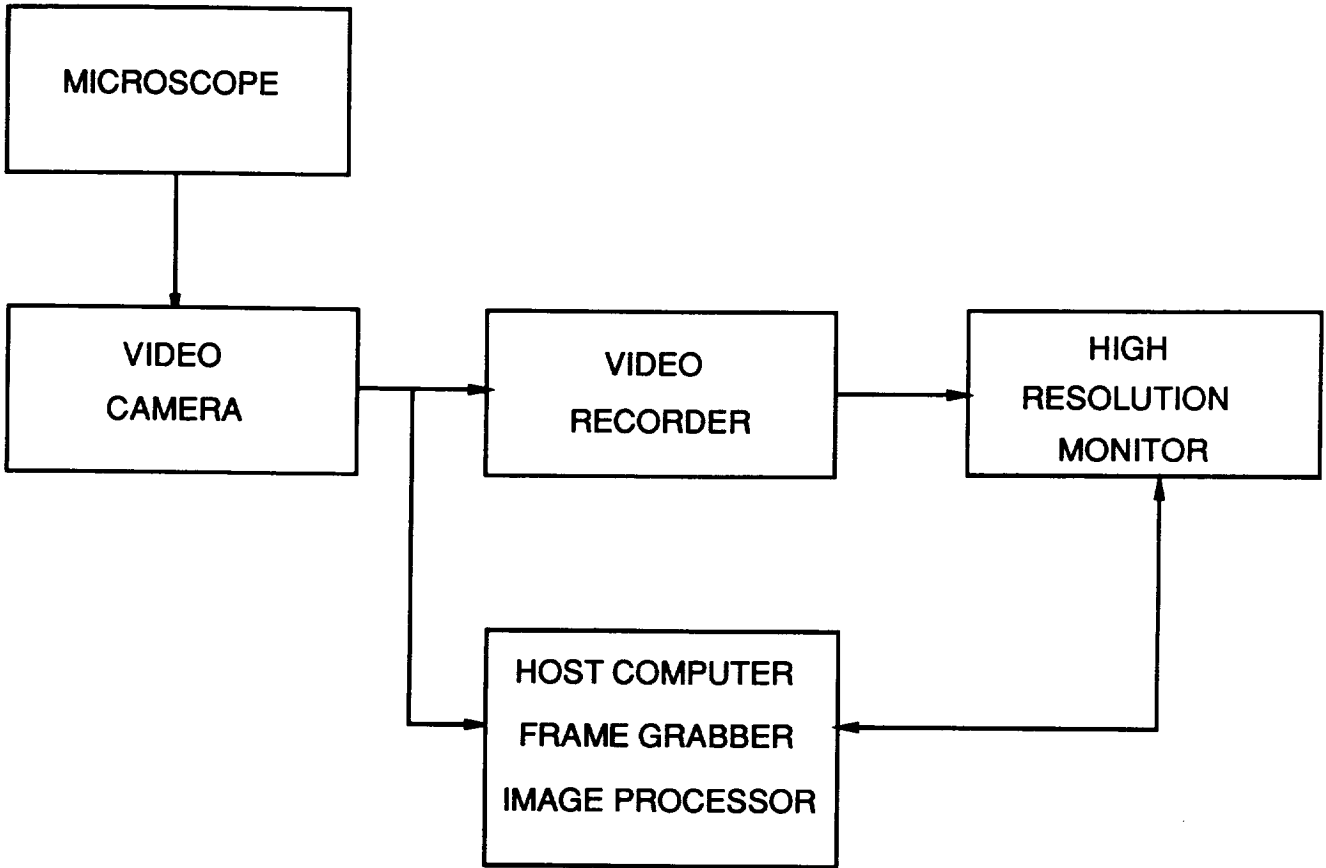


FIG. 22

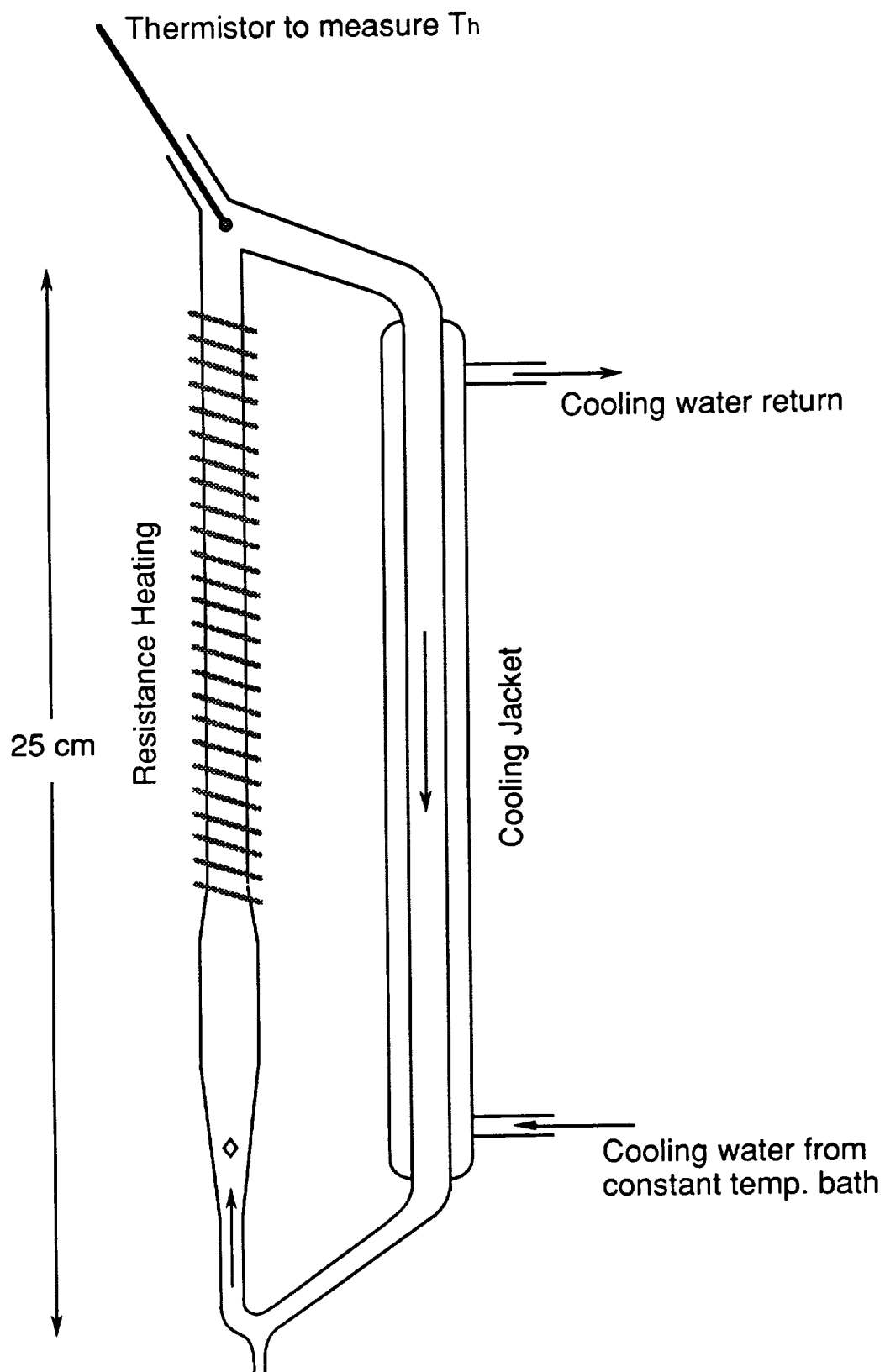


FIG. 23

10. Presentations and Publications of Research under this Grant

F. Rosenberger; Solubility Studies and Their Use in Protein Crystallization Control; invited presentation at Forty-fifth Pittsburgh Diffraction Conference, Charlottesville, Virginia, November 1987.

T. A. Nyce; Temperature Control of Crystallization and Convection as a Possible Cause for Growth Cessation; presented at Third International Conference on the Crystallization of Biological Macromolecules, Washington D. C., August 13-19, 1989.

T. A. Nyce and F. Rosenberger; Growth of Protein Crystals Suspended in a Closed Loop Thermosyphon; *J. Crystal Growth* (in print);

J. D. Fehribach and F. Rosenberger; Analysis of Models for Two Solution Crystal Growth Problems; *J. Crystal Growth* 94 (1989) 6.

F. Rosenberger; Microgravity Materials Research in the U. S.; invited presentation at Ninth International Conference on Crystal Growth; Sendai, Japan, August 20-25, 1989.

T. A. Nyce; Novel Protein Crystal Growth Technology; presentation at Third Annual Alabama Materials Research Conference, Huntsville, Alabama, September 20-21, 1989.

T. A. Nyce; Temperature Control of Nucleation and Growth of Protein Crystals; presentation at New Developments in Protein Crystal Growth Workshop, Gulf Shores, Alabama, May 11-14, 1990.

L. Monaco, N.-B. Ming and F. Rosenberger; High Resolution Microscopy of Lysozyme-Solution Interfaces; poster at New Developments in Protein Crystal Growth Workshop, Gulf Shores, Alabama, May 11-14, 1990.

T. A. Nyce and F. Rosenberger; General Method for Calculating Velocities and Heat Transfer in Closed Loop Natural Convection Systems; submitted to *International Journal of Heat and Mass Transfer*.

T. A. Nyce; Temperature Control of Nucleation and Growth of Protein Crystals; presentation at Eighth American Conference on Crystal Growth, Vail, Colorado, July 15-20, 1990.

F. Rosenberger; Protein Crystal Growth; invited presentation at NASA Microgravity Fluids Workshop; Cleveland, Ohio, August 7-9, 1990.

11. Attachments

J. D. Fehribach and F. Rosenberger, Analysis of Models for Two Solution Crystal Growth Problems, *J. Crystal Growth* 94 (1989) 6.

T. A. Nyce and F. Rosenberger, Growth of Protein Crystals Suspended in a Closed Loop Thermosyphon, *J. Crystal Growth* (in print).

T. A. Nyce and F. Rosenberger, General Method for Calculating Velocities and Heat Transfer in Closed Loop Natural Convection Systems, submitted to *International Journal of Heat and Mass Transfer*.

ANALYSIS OF MODELS FOR TWO SOLUTION CRYSTAL GROWTH PROBLEMS

Joseph D. FEHRIBACH

Department of Mathematics and Statistics, University of Alabama at Huntsville, Huntsville, Alabama 35899, USA

and

Franz ROSENBERGER

Center for Microgravity and Materials Research, University of Alabama at Huntsville, Huntsville, Alabama 35899, USA

Received 10 May 1988; manuscript received in final form 17 August 1988

Two diffusive solution crystal growth models are considered in which transport is governed by small parameters. The first is a simple model describing precipitant-driven solution crystal growth; the second describes a hanging drop evaporation configuration used for protein crystallization. Both contain components with widely differing diffusivities, the ratio being ϵ . The second system also has a small density ratio ρ between the two contacting phases. Asymptotic scaling methods are used to show that in the first problem, the precipitant concentration remains uniform to $O(\sqrt{\epsilon})$, while in the second, the drop concentrations remain uniform to $O(\rho/\sqrt{\epsilon})$ if $\rho \ll \sqrt{\epsilon}$ and the vapor concentrations remain uniform to $O(\sqrt{\epsilon}/\rho)$ if $\sqrt{\epsilon} \ll \rho$. The latter result implies that the drop will remain effectively well mixed when $\rho \ll \sqrt{\epsilon}$, but that sharp gradients will develop in the drop when $\sqrt{\epsilon} \ll \rho$. An example is given to indicate that for certain proteins, sharp concentration gradients may develop in the drop during evaporation, while under the same conditions, the concentrations of other proteins remain uniform.

1. Introduction

Small parameters play important roles in many physical systems, solution crystal growth processes being no exception. Two such situations often occurring in protein crystallization are considered here. The first model describes precipitant-driven solution crystal growth, and the second describes a hanging drop evaporation problem. Both models have several features in common: (1) two phases separated by an interface (a free boundary), (2) no convective mixing in either phase, and (3) diffusion components with widely differing diffusivities. (The lack of convective mixing implies that the models are formulated for low gravity conditions.) In addition, in the second model the ratio of the density of the contacting phases is small. We will show that the ratio of the diffusivities and that of the densities are the small parameters which are critical in determining the concentration profiles and the interface velocity.

The first model is a simple, one-dimensional model of the growth of a pure crystal from a liquid phase containing both the solute (protein) and a salt (precipitant) in a solvent (see fig. 1a). The interface separating the solid and liquid phases is assumed to be planar, and the initial concentrations in the liquid phase are assumed to be spatially uniform. Although this model is very simple, it does exhibit several interesting phenomena which have implications for solute crystal growth processes in general.

The second model describes a hemispherical drop containing solute (protein) and solvent (water) suspended over a hemispherical desiccant well (see fig. 1b). The initial concentration of protein in the drop (again assumed uniform) is such that water evaporates from the drop and is absorbed by the well.

Let ϵ be the small ratio of the diffusivities in each of these problems (protein to precipitant for the first, protein in the drop to vapor in the gap

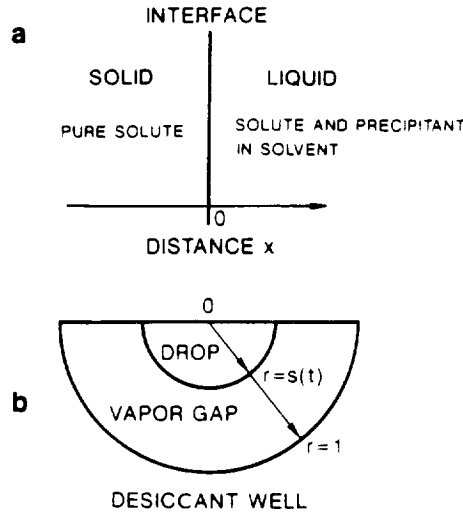


Fig. 1. Defining sketches for problems treated: (a) precipitant-driven solution growth; (b) hanging drop crystallization technique. Drop: water and protein; vapor gap: water vapor in air.

for the second). Let ρ be the ratio of the density of the damp air in the gap to the density of the drop. It will be shown that:

(a) there is a concentration boundary layer with thickness $O(\sqrt{\epsilon})$ at the interface in the concentration profile of the less diffusive component (this is a well-known result);

(b) in the first model, the interface velocity is $O(\sqrt{\epsilon})$; in the second, this velocity is either $O(\sqrt{\epsilon})$ or $O(\rho)$ depending on the relative size of the two parameters;

(c) in the first model, the change in precipitant concentration from its initial value is $O(\sqrt{\epsilon})$; in the second, for $\sqrt{\epsilon} \ll \rho$, the change in vapor concentration from its initial value is $O(\sqrt{\epsilon}/\rho)$, while for $\sqrt{\epsilon} \gg \rho$, the change in protein concentration from its initial value is $O(\rho/\sqrt{\epsilon})$.

Result (c) has several important physical consequences. For the first problem, it implies that the precipitant concentration will remain uniform and that the protein concentration will adjust to satisfy the interface conditions. For the second problem, since there are proteins for which $\sqrt{\epsilon} < \rho$ and others for which $\sqrt{\epsilon} > \rho$, result (c) indicates that for some proteins the hanging drop will remain effectively well mixed, even in the absence of

convection, while for others a sharp gradient may develop in the protein concentration of the drop if no convection is assumed.

Mathematically, these two models are particular cases of a class of problems known as Stefan problems [1,2]. (The mass conservation interface conditions given below are often referred to as Stefan conditions.) They are also related to alloy solidification problems (ref. [1], pp. 14–16) and to models of solid diffusion where ϵ is the small solid diffusivity (cf. refs. [3,4] and their references).

In sections 2 and 3, respectively, models for the protein-precipitant problem and the hanging drop problem are examined mathematically. In both cases numerical examples are given to illustrate the results.

2. A simple model for precipitant-driven, diffusion-controlled crystal growth

Consider the following one-dimensional, semi-infinite system of differential equations ($p = p(x, t)$, $n = n(x, t)$, $v = v(t)$, and subscripts denote partial derivatives):

$$p_t = \epsilon p_{xx} + vp_x, \quad 0 < x < \infty, \quad t > 0, \quad (1a)$$

$$n_t = n_{xx} + vn_x, \quad 0 < x < \infty, \quad t > 0, \quad (1b)$$

$$v(1-p) = \epsilon p_x, \quad x = 0, \quad t > 0, \quad (1c)$$

$$-vn = n_x, \quad x = 0, \quad t > 0, \quad (1d)$$

$$F(n, p, T) = 0, \quad x = 0, \quad t > 0, \quad (1e)$$

$$p(x, 0) = p_\infty, \quad 0 < x < \infty, \quad (1f)$$

$$n(x, 0) = n_\infty, \quad 0 < x < \infty. \quad (1g)$$

This system can be viewed as a simple model for precipitant-driven protein crystal growth from a liquid phase (fig. 1a) for the initial time period when the liquid can be considered semi-infinite. Let $p(x, t)$ be the concentration of protein and let $n(x, t)$ be the concentration of precipitant in the liquid which at time $t = 0$ is placed in contact with a solid protein. Both concentrations are measured in mole fractions. The solid-liquid interface is assumed planar, and the reference frame moves with the interface (i.e., the location of the interface

is always at $x = 0$). Recall that ϵ is the ratio of the protein diffusivity to the precipitant diffusivity. Typically for protein-precipitant problems $10^{-3} < \epsilon < 10^{-1}$. Finally the temperature T is a known constant or function of time, and $v(t)$ is the velocity of the moving interface.

The two equations, (1a) and (1b), for the liquid phase represent simple Fickian diffusion in the moving reference frame. The first two interface conditions, (1c) and (1d), ensure mass conservation of protein and precipitant across the interface, while the third condition, (1e), relates the protein and precipitant concentrations which are in equilibrium in the solvent at the temperature T . Finally p_∞ and n_∞ are constants giving the uniform initial concentrations of protein and precipitant in the liquid phase.

In this model, $p(x, t)$, $n(x, t)$ and $v(t)$ are a priori unknown functions to be determined by the system (1). Though it is not possible to explicitly solve for these functions when temperature varies with time, it is possible to analyze the system to determine how they depend on the parameter ϵ . The main tool in the analysis of system (1) is the method of *dominant balance*. As its name implies, this method determines the qualitative characteristics of the solution of a system of differential equations by determining the dominant (i.e., largest, most important) terms in the system, then balancing these terms while ignoring the smaller, less important terms (cf. ref. [5], p. 83ff). Here dominant balance will be used to eliminate the parameter ϵ from (1) and thereby establish the conclusions mentioned in the introductory section.

Consider first the differential equation for the protein in the liquid, and define a new spacial variable $X \equiv x/\epsilon^r$. One wishes to choose r to balance the terms in this equation with respect to their dependence on ϵ . In finding this balance, one is finding the natural length scale for this equation. In terms of X , (1a) becomes

$$p_t = \epsilon^{1-2r} p_{XX} + v \epsilon^{-r} p_X. \quad (2)$$

Near the interface the appropriate scaling will be given by either $r = 1/2$ or $r = 1$ depending on whether the motion of the interface is governed by

diffusion or by some other driving force. When $r = 1$, eq. (2) becomes

$$p_t = \frac{1}{\epsilon} p_{XX} + \frac{v}{\epsilon} p_X.$$

This value of r gives the finest scaling and is appropriate for rapid growth, i.e., provided the velocity is $O(\epsilon^0)$ (large compared to ϵ). With $r = 1/2$, however, eq. (2) becomes

$$p_t = p_{XX} + \frac{v}{\sqrt{\epsilon}} p_X.$$

This is the appropriate scaling for diffusion controlled growth where $v = O(\sqrt{\epsilon})$. Here all terms are $O(\epsilon^0)$.

To determine whether the growth is rapid or diffusion controlled, one must analyze the interface conditions, (1c), (1d) and (1e). Consider first the limit in which there is no protein diffusion, i.e., $\epsilon \rightarrow 0$. The interface conditions are then

$$v(1-p) = 0, \quad -vn = n_\infty, \quad F(n, p, T) = 0.$$

Direct substitution confirms that this system has a unique solution: $v(t) \equiv 0$, $n(x, t) \equiv n_\infty$, and $p(0, t)$ chosen so that $F(n_\infty, p(0, t), T) = 0$. Note that neglecting the protein diffusivity leads to a discontinuity in the protein profile: $p(0, t)$ is determined by F while $p(x, t) \equiv p_\infty$ for $x > 0$ from the initial condition (1f).

The above solution implies that in the absence of diffusion, the interface does not move; there are no other forces driving the interface in this model. Therefore the appropriate scaling for this model near the interface is the coarser $r = 1/2$ scaling. Rewriting the original interface conditions in terms of this scaling, one finds

$$v(1-p) = \sqrt{\epsilon} p_X, \quad (3a)$$

$$v(-n) = n_\infty, \quad (3b)$$

$$F(n, p, T) = 0. \quad (3c)$$

Since $1-p$ is $O(\epsilon^0)$ (i.e., large with respect to ϵ), eq. (3a) is consistent with $v = O(\sqrt{\epsilon})$. But considering (3b), $v = O(\sqrt{\epsilon})$ implies that $n_\infty = O(\sqrt{\epsilon})$. That is to say, the gradient in the precipitant profile is shallow near the interface. Together with (1b) and the initial condition $n(x, 0) = n_\infty$, this shallow

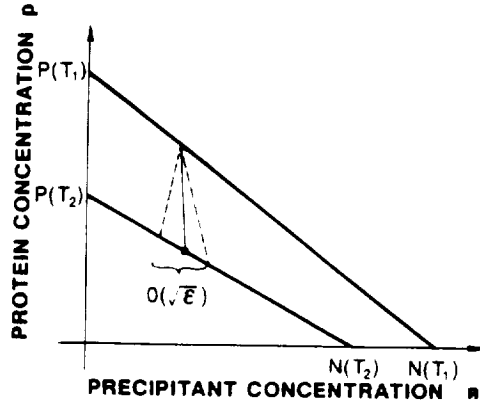


Fig. 2. Linear equilibrium (solubility) relations for two temperatures. $P(T)$ and $N(T)$ are defined in the text.

gradient implies that $|n(x, t) - n_\infty| = O(\sqrt{\epsilon})$ for all (x, t) .

This last point also has an interesting implication regarding how the interface concentrations change with temperature. Since the interface concentrations are required to be in equilibrium (i.e., lie on the coexistence line of the phase diagram), and since $|n(x, t) - n_\infty| = O(\sqrt{\epsilon})$, the interface protein concentration must adjust to changes in temperature (see fig. 2).

We have generated numerical plots of protein and precipitant concentrations for two proteins, myosin and lysozyme. These particular proteins were chosen because their diffusivities ($D_{my} = 1.1 \times 10^{-7} \text{ cm}^2/\text{s}$ and $D_{ly} = 10.4 \times 10^{-7} \text{ cm}^2/\text{s}$ [6]) represent opposite extremes for proteins typically used in crystal growth experiments [7]. The precipitant used here is NaCl ($D_{NaCl} = 1.6 \times 10^{-5} \text{ cm}^2/\text{s}$). Because of the general lack of detailed knowledge of the phase diagrams of most proteins, a generic, linear solubility relation is used for (1e) in these examples. Realistic solubility relations (where available, see, e.g., ref. [8] for lysozyme) show qualitatively the same parameter dependence.

For these illustrations, assume that temperature is given by (see fig. 3):

$$T(t) = \begin{cases} T_0, & 0 \leq t \leq t_0, \\ T_0 - \alpha(t - t_0), & t_0 \leq t. \end{cases}$$

The temperature is assumed constant for small

times to avoid numerical stiffness problems (see below). Also assume a linear solubility relation (see fig. 2):

$$\frac{p}{P(T)} + \frac{n}{N(T)} = 1,$$

where $P(T)$ and $N(T)$ are defined as

$$P(T) = \kappa(1 + \tan^{-1}(2T)),$$

$$N(T) = (0.1)(1 + \tan^{-1}(3T)).$$

The constant κ depends on the protein. Though this solubility relation was chosen mainly for computational convenience, it does yield typical protein and precipitant mole fractions and qualitatively does reflect the temperature dependence of the solubility relation.

Figs. 4 and 5 were generated with an analytical-numerical scheme due to Small and Ghez [3]. Since the system (1) assumes rapid surface kinetics, the interface velocity and the concentration gradients are initially infinite. Therefore the system is numerically stiff during the initial period. Since the temperature is constant during this period, however, (1) can be reduced to an ordinary differential system in the variable $\xi = x/2\sqrt{t}$. The solution to this system, called a similarity solution, can be used until time $t = t_0$. After this time, (1) can be solved numerically; in this case an explicit finite difference scheme is sufficient.

Fig. 4 shows the protein and precipitant profiles in the solution for lysozyme and NaCl ($\epsilon = 6.5 \times 10^{-2}$) at several times, three at T_0 and two during the temperature ramping. The initial concentrations (in mole fractions) are $p_\infty = 0.0008$

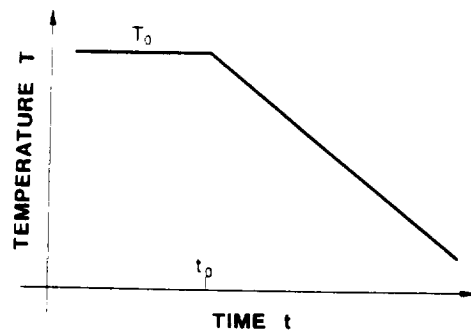


Fig. 3. Temperature function used.

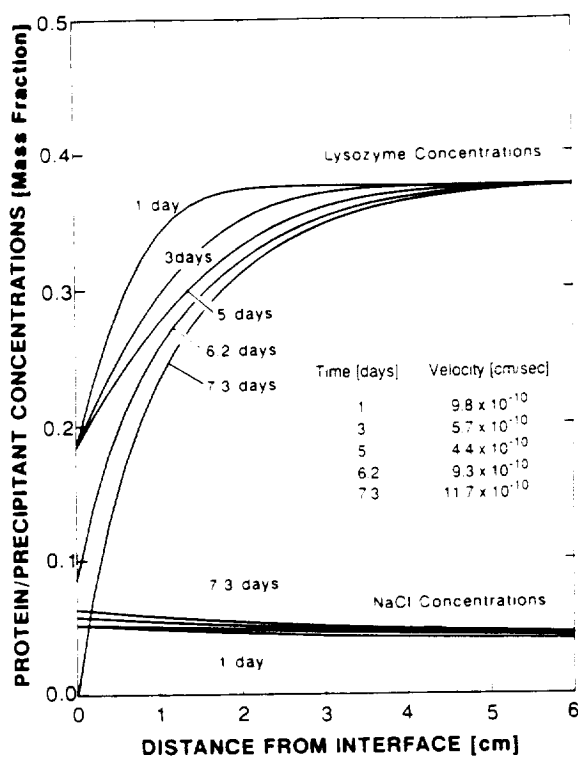


Fig. 4. Calculated concentration profiles for lysozyme-NaCl system at various times. $\epsilon = 6.5 \times 10^{-2}$. Inset table shows instant growth velocities corresponding to growth times given.

and $n_\infty = 0.02$, $\kappa = 0.001$, and for the temperature profile $T_0 = 0$, $t_0 = 5$ days and $\alpha = 0.1 \text{ day}^{-1}$. Note that the plot is in mass fractions so that the protein and salt concentrations can be compared on a convenient scale. The interface concentrations do not change while the temperature is constant, but the protein interface concentration changes noticeably during the ramp. The sequence of plots shows the development of a protein concentration boundary layer in contrast to the small changes in the precipitant concentration from its initial value. The corresponding instantaneous interface (growth) velocities are also given on the figure. Note that these velocities are ten to one hundred times slower than experimentally measured values [9]. This difference is due mainly to the model assumption that the crystal is pure protein. Real protein crystals incorporate water during growth, and some contain as much as fifty percent salt water by volume. Consequently the

mole fraction of protein in the crystal may be as low as 0.001. Using this protein mole fraction value for the crystal in (1), particularly (1c), would increase the growth rate by up to three orders of magnitude. To a lesser extent, the growth rate is also affected by the presence of convection in the laboratory experiments.

Fig. 5 shows five similar plots for myosin and NaCl ($\epsilon = 6.9 \times 10^{-3}$). For this plot, $p_\infty = 0.0004$, $n_\infty = 0.02$, $\kappa = 0.0002$ and the temperature profile parameters are the same as before. Note the decrease in interface velocity, the narrowing of the boundary layer, and the relatively smaller change in the precipitant concentration. To the authors' knowledge, growth rates for myosin have not been measured, but these are again slower than what one would expect.

By way of comparison it is interesting to consider a case where ϵ is large, say $\epsilon = 0.2$ (note that the numerical computations do not require that ϵ

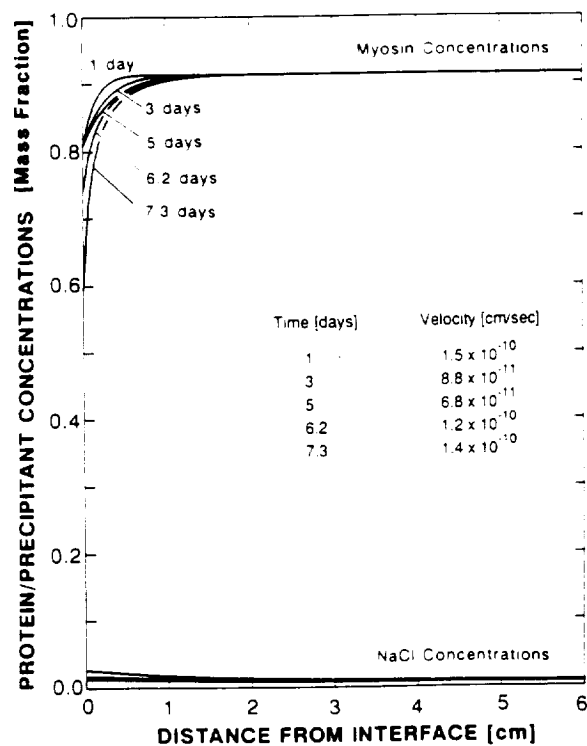


Fig. 5. Calculated concentration profiles for myosin-NaCl system at various times. $\epsilon = 6.9 \times 10^{-3}$. Inset table shows instant growth velocities corresponding to growth times given.

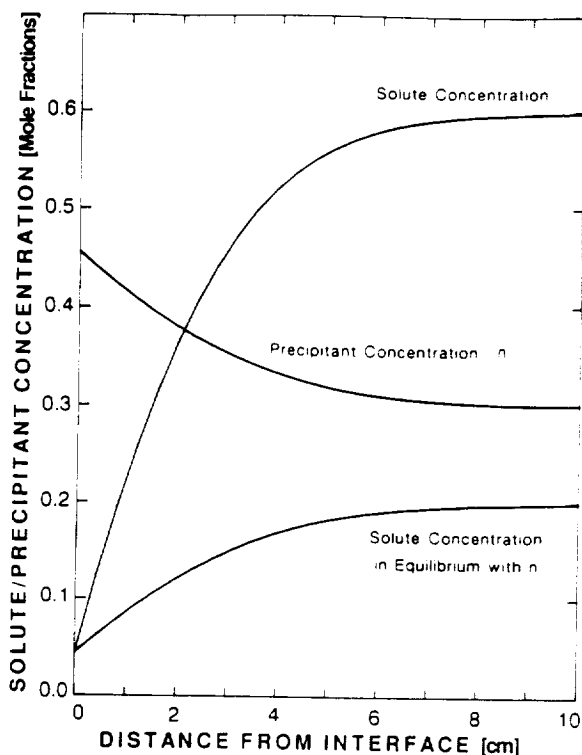


Fig. 6. Calculated concentration profiles for system with comparable diffusivities of solute and precipitant after $t = 5$ days. $\epsilon = 0.2$.

be small). Keep in mind that this value does not correspond to a protein-precipitant system, but it may occur in other solution growth processes. Fig. 6 shows p and n profiles for $\epsilon = 0.2$ with NaCl as the precipitant at $t = 5$ days using the simple solubility relation $p + n = 1/2$; note that the temperature is now constant. A curve showing what solute concentration, p_{eqn} , would be in equilibrium with n is included to indicate the supersaturation in the liquid phase. Note that the presence of the precipitant decreases the magnitude of the supersaturation away from the interface, as compared to a solely temperature driven growth process where p_{eqn} is constant throughout. This decrease has implications for the morphological stability of the phase interface, viz., the decreased interface supersaturation gradient may give stability to a planar interface that would be unstable in the absence of the precipitant.

3. The hanging drop

The hanging drop problem (fig. 1b) is mathematically quite similar to the problem considered in the previous section. The system of differential equations derived for this problem is

$$u_t = \epsilon \frac{1}{r^2} (r^2 u_r)_r, \quad u + w = 1, \quad 0 < r < s(t), \quad (4a)$$

$$u \equiv 0, \quad w_t = \frac{1}{r^2} (r^2 w_r)_r, \quad s(t) < r < 1, \quad (4b)$$

$$v u^- = -\epsilon (u_r)^-, \quad r = s(t), \quad (4c)$$

$$v (w^+ - w^-) = \epsilon (w_r)^- - \rho (w_r)^-, \quad r = s(t), \quad (4d)$$

$$F(w^+, w^-, T) = 0, \quad r = s(t), \quad (4e)$$

$$u(r, 0) = u_0, \quad 0 < r < s(0), \quad (4f)$$

$$w(r, 0) = w^{eq}, \quad s(0) < r < 1, \quad (4g)$$

$$u_r(0, t) = 0, \quad t > 0, \quad (4h)$$

$$w(1, t) = w^{eq}, \quad t < 0. \quad (4i)$$

Here $u = u(r, t)$ is the protein concentration, $w = w(r, t)$ is the water concentration (again in mole fractions), and $s = s(t)$ is the position of the interface. The superscripts $+$ and $-$ denote limits taken from the positive and the negative sides of the interface respectively. The center of the drop is at $r = 0$; the edge of the desiccant well is at $r = 1$. The factor ρ is the ratio of the density of damp air to that of the drop. The parameter ϵ is the ratio of the diffusivity of protein in the drop to the diffusivity of vapor in the gap between the drop and the well. Here the function F is obtained from the coexistence curve that relates the concentrations of water vapor and liquid water which are in equilibrium at temperature T .

The model is reduced to being effectively one-dimensional by assuming that the problem remains radially symmetric for all time. As in the previous model, the differential equations (4a) and (4b) represent Fickian diffusion, but now in a radial coordinate. That $u(r, t) + w(r, t) \equiv 1$ for $r < s(t)$ simply says that the drop contains only protein and water; that $u(r, t) \equiv 0$ for $r > s(t)$

implies that there is no protein in the gap. Eqs. (4c) and (4d) represent mass conservation across the surface of the drop (for a careful derivation of this type of condition, cf. ref. [3], p. 5324). Eq. (4h) states that no water radially crosses the upper boundary at the center of the drop. Physically, this is the poorest assumption since the vertical derivative rather than the radial derivative should be zero. The more physically realistic assumption, however, would break the radial symmetry of the system, and hence shall not be assumed here. Eq. (4i) implies that the vapor concentration at the surface of the well is always in equilibrium with the well. Since the well is a perfect reservoir, this equilibrium concentration w^{eq} is constant in time. Finally note that density changes in the vapor phase can be neglected since the interface motion is very slow relative to diffusion across the gap.

It should be particularly noted that this model assumes that there is no convection in the drop. This assumption is appropriate only for microgravity environments and in the absence of surface tension driven flow. A model where the drop is assumed perfectly (convectively) mixed has been given by Baird et al. [10].

Using $u = 1 - w$ inside the drop, system (4) can be written entirely in terms of the water concentration. Also the system can be transformed into a reference frame which moves with the interface by replacing r by $z \equiv r - s(t)$. Making these substitutions and performing several algebraic manipulations, one finds

$$w_t = \epsilon \frac{1}{z^2} (z^2 w_z)_z + v w_z, \quad -s(t) < z < 0, \quad (5a)$$

$$w_t = \frac{1}{z^2} (z^2 w_z)_z + v w_z, \quad 0 < z < 1 - s(t), \quad (5b)$$

$$v(1 - w^-) = \epsilon (w_z^-), \quad z = 0, \quad (5c)$$

$$v(1 - w^+) = \rho (w_z^+), \quad z = 0, \quad (5d)$$

$$F(w^+, w^-, T) = 0, \quad z = 0, \quad (5e)$$

$$w(z, 0) = w_0, \quad -s(t) < z < 0, \quad (5f)$$

$$w(z, 0) = w^{\text{eq}}, \quad 0 < z < 1 - s(t), \quad (5g)$$

$$w_z(0, t) = 0, \quad t > 0, \quad (5h)$$

$$w(1, t) = w^{\text{eq}} \quad t > 0. \quad (5i)$$

System (5) is now much like system (1), and the method of dominant balance is again applicable. As before, when diffusion in the drop is ignored, the interface conditions can be solved, viz., $v(t) = 0$, $w^-(0, t) \equiv w^{\text{eq}}$, and w^+ given implicitly by $F(w^+, w^{\text{eq}}, T) = 0$. Therefore diffusion inside the drop is the force driving the motion of the interface, and the entire system can be written using the scaling $Z = z/\sqrt{\epsilon}$. Interface conditions (5c) and (5d) then become

$$v(1 - w^-) = \sqrt{\epsilon} (w_z^-), \quad (6a)$$

$$v(1 - w^+) = \rho (w_z^+), \quad (6b)$$

From (6) it follows that the parameter dependence of the interface velocity and the concentration profiles is determined by the relative sizes of $\sqrt{\epsilon}$ and ρ . Suppose first that $\sqrt{\epsilon} \ll \rho$. Then (6a) implies that $v = O(\sqrt{\epsilon})$, and (6b) implies $(w_z^+)^- = O(v/\rho) = O(\sqrt{\epsilon}/\rho)$. So in the gap $|w(r, t) - w^{\text{eq}}| = O(\sqrt{\epsilon}/\rho)$ (i.e., the change in the vapor concentration is small) and the protein concentration in the drop must adjust to satisfy the equilibrium condition (5e). Now on the other hand, suppose that $\rho \ll \sqrt{\epsilon}$. Then (6b) implies that $v = O(\rho)$, and (6a) implies that $(w_z^-)^- = O(\rho/\sqrt{\epsilon})$. So in this case the vapor concentration in the gap must adjust to satisfy (5e).

To illustrate this result, consider the numerical plots for lysozyme and a hypothetical, myosin-like protein show in fig. 7. This example was brought to the authors' attention by A. Nadarajah of our Center. A similar example has also been discussed by Grant [11]. The plots were made for system (5) for large times assuming a steady state concentration profile in the gap, using an explicit finite difference scheme in the drop, and using a three point difference scheme to evaluate the drop gradient at the interface. The hypothetical protein is assumed to have the diffusivity of myosin, but in other regards to be like lysozyme. Hence the equilibrium coexistence curve (5e) for both proteins is that of lysozyme. For the concentration range considered here at $T = 25^\circ\text{C}$, this curve is given by

$$1 = 9.304 w^- - 265.66 w^+.$$

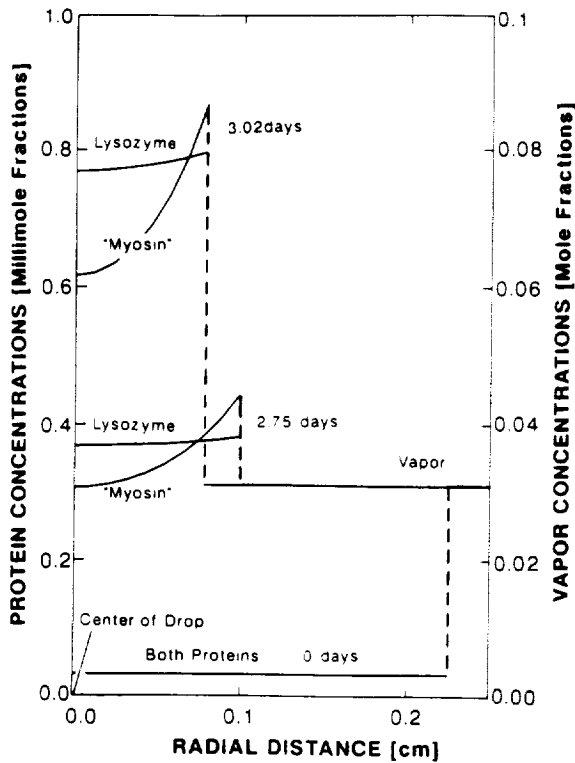


Fig. 7. Calculated concentration profiles in hanging drop system at three times: 0, 2.75 and 3.02 days. The dashed connecting lines represent the positions of the drop-vapor interface. For lysozyme the ratio $Q = 0.56$, and the protein concentration remains uniform. For the myosin-like protein, $Q = 1.72$, and a sharp protein concentration gradient develops in the drop.

The curve was derived assuming the protein solution is ideal and using Raoult's Law [12]. For lysozyme $\epsilon = 4.00 \times 10^{-6}$ ($D_{\text{vapor}} = 0.26 \text{ cm}^2/\text{s}$ ($\text{H}_2\text{O}:\text{air}$), $D_{\text{ly}} = 10.4 \times 10^{-7} \text{ cm}^2/\text{s}$); for myosin $\epsilon = 4.23 \times 10^{-7}$ ($D_{\text{m}_v} = 1.1 \times 10^{-7} \text{ cm}^2/\text{s}$). The gap radius is 1.2 cm and the initial drop radius is 0.23 cm (hence the normalized initial interface position is $s(0) = 0.19$). The other parameter values for both proteins are $w_0 = 0.999968$, $w^{\text{eq}} = 0.0311$, and $\rho = 1.12 \times 10^{-3}$ ($\rho_{\text{vapor}} = 1.14 \times 10^{-3} \text{ g/cm}^3$, $\rho_{\text{drop}} = 1.02 \text{ g/cm}^3$ [13]). All of these are typical values for protein hanging drop evaporation experiments [7].

For convenience, define the dimensionless ratio $Q \equiv \rho/\sqrt{\epsilon}$. This ratio measures the relative contributions of the diffusivities and densities in determining the qualitative shape of the concentra-

tion profiles. For $Q \ll 1$, $\rho \ll \sqrt{\epsilon}$, and the drop concentrations are flat. For $Q \gg 1$, $\rho \gg \sqrt{\epsilon}$, and the vapor concentrations are flat. For proteins, however, the range of Q -values straddles unity ($Q_{\text{ly}} = 0.56$, $Q_{\text{m}_v} = 1.72$). Hence one might expect qualitatively different profiles for proteins at the opposite ends of this range. Fig. 7 shows this to be the case. The myosin-like protein profiles steepen, while the lysozyme profiles remain relatively flat. The vapor concentrations are flat for both proteins for all times. After roughly 3.6 days both drops equilibrate, i.e., due to the increased protein concentration the water vapor pressure at the drop surface is reduced to w^{eq} of the well, whence evaporation ceases and the protein concentrations again become uniform.

In actual experiments, salt is a precipitating agent for the protein in the drop, and since the mole fraction of protein is negligible compared to that of salt, the evaporation rate is controlled by the salt concentration. However, for a fixed salt concentration (since $Q_{\text{salt}} \approx 0.15$, the salt concentration will remain uniform), the Q -value for a protein still measures the steepness of its concentration gradient.

The steepening profiles illustrated in fig. 7 have significant implications for the possible development of convective instabilities in the drop. It should be kept in mind, though, that since protein Q -values are close to unity, physical effects not considered in this model could substantially effect the qualitative character of protein profiles in laboratory experiments. One would expect the profiles to be very sensitive to how the experiment is performed.

Acknowledgements

We wish to thank Arunan Nadarajah, Ed Meehan and Pam Twigg for many helpful discussions and for obtaining the parameter values used here. Also support of this research by the Microgravity Science and Applications Division of the National Aeronautics and Space Administration under Grant NAG8-711 and by the State of Alabama is gratefully acknowledged.

References

- [1] J. Crank, *Free and Moving Boundary Problems* (Clarendon, Oxford, 1984).
- [2] J.R. Ockendon, in: *Moving Boundary Value Problems in Heat Flow and Diffusion*, Eds. J.R. Ockendon and W.R. Hodgkins (Clarendon, Oxford, 1974).
- [3] M.B. Small and R. Ghez, *J. Appl. Phys.* 50 (1979) 5322.
- [4] J.D. Fehribach, *SIAM J. Math. Anal.* 19 (1988) 86.
- [5] C.M. Bender and S.A. Orszag, *Advanced Mathematical Methods for Scientists and Engineers* (McGraw-Hill, New York, 1978).
- [6] C.R. Cantor and P.R. Schimmiel, *Biophysical Chemistry, Part II: Techniques for the Study of Biological Structural and Function* (Freeman, San Francisco, 1980) p. 584.
- [7] E.J. Meehan and P.J. Twigg, personal communications.
- [8] S.B. Howard, P.J. Twigg, J.K. Baird, E.J. Meehan, *J. Crystal Growth* 90 (1988) 94.
- [9] M. Pusey and R. Naumann, *J. Crystal Growth* 76 (1986) 593.
- [10] J.K. Baird, R.W. Frieden, E.J. Meehan, Jr., P.J. Twigg, S.B. Howard and W.W. Fowles, *Mater. Res. Soc. Symp. Proc.* 87 (1987) 231.
- [11] M.L. Grant, paper presented at the Joe Wheeler Protein Crystal Growth Workshop, May 1988.
- [12] J.M. Smith and H.C. Van Ness, *An Introduction to Chemical Engineering Thermodynamics*, 3rd ed. (McGraw-Hill, New York, 1975) pp. 296–302.
- [13] W.W. Fowles, L.J. DeLucas, P.J. Twigg, S.B. Howard, E.J. Meehan, Jr. and J.K. Baird, *J. Crystal Growth* 90 (1988) 117.

**GROWTH OF PROTEIN CRYSTALS SUSPENDED IN A
CLOSED LOOP THERMOSYPHON**

Thomas A. Nyce and Franz Rosenberger

Center for Microgravity and Materials Research
University of Alabama in Huntsville
Huntsville, Alabama 35899

ABSTRACT

The quality of protein crystals often suffers from their growth at a liquid or solid surface. A novel solution growth method was developed to alleviate this problem. A growing crystal is suspended in a specially configured upflow of supersaturated nutrient, which is provided by the effect of fluid buoyancy in a closed loop thermosyphon. The flow rate and supersaturation are controlled by the temperature distribution in the thermosyphon, while contact of the crystal with the wall during growth is practically eliminated. The method was applied to the growth of lysozyme single crystals, with surprising results. While the orthorhombic form of lysozyme grew readily to the suspension limit of this particular apparatus (1.5 mm), the tetragonal form grew only to a maximum size less than 0.1 mm. Seed crystals of tetragonal lysozyme introduced into stagnant batch controls did not experience the growth cessation that the suspended crystals did. A possible cause of this growth cessation is the fluid shear forces on the suspended crystals.

1. Introduction

The goal of this research was to develop a new technology for solution crystal growth in which crystals are freely suspended in the nutrient solution, eliminating container wall or seed holder contacts and maximizing the uniformity in solute supply to the interface. In particular, the applicability of this technology to the growth of protein crystals was to be explored. The basic idea is to suspend a growing crystal in a specially configured upflow of supersaturated nutrient where the upflow is provided by the effect of fluid buoyancy in a closed loop thermosyphon.

The physical size and temperature distribution of a thermosyphon needed to generate the suspension velocities required to balance the settling velocities of desired crystal sizes were estimated. A specially shaped expansion chamber was designed to keep the crystals suspended in a stable position in the center of the flow. Additionally an operating procedure was developed which included a startup sequence to trap and suspend nuclei or seeds in the expansion chamber and allows for the later reduction of the number of crystals in the chamber.

2. Design of the apparatus

2.1 Particle Suspension Dynamics

The primary design quantity is the suspension velocity required to accommodate the crystals as they grow. When this upward velocity is equal to the rate at which the crystal would settle in a motionless fluid, the crystal will remain suspended. The evaluation of settling rates for nonspherical particles such as faceted crystals of various shapes, however, is not well established. Hence, the calculations for suspension velocities gave only general guidelines and actual experimental trials were relied on heavily.

The interaction between a spherical particle of diameter D in a fluid of kinematic viscosity ν and relative velocity U is governed by the particle Reynolds number $Re_p = DU/\nu$. If $Re_p < 0.03$ Stoke's law can be used for the calculation of settling velocities [1]. For the settling of larger spherical particles, i.e. in the "intermediate law" region, see [2]. Note that the drag experienced by nonspherical particles depends sensitively on their specific shape and their orientation with respect to the direction of motion. Guidelines for determining the orientation in free fall as a function of the particle Reynolds number (based on the diameter of a sphere of equal surface area) are given by Becker [3]. Since the shapes of crystals of a given material can vary widely depending on the growth conditions, experiments must be relied on for the determination of the "falling" orientation and the required suspension velocity.

It must be noted that the above correlations are for bodies settling in a free fluid with no walls. If, however, a particle is settling in a tube, the presence of a wall increases the drag on the particle [4] and thus reduces the upward velocity required to suspend it. For instance, if the

particle diameter is 10% of the tube diameter, its settling velocity is 20% less than in an infinite fluid and the pressure distribution in the annular space will tend to center the particle.

2.2 Design of the Expansion Chamber

The design of the expansion chamber (fig. 1) itself is critical. The velocity in the smallest part of the chamber must be large enough to suspend the largest crystal size desired and the velocity in the largest part must be small enough to trap nuclei or seed crystals of a very small size. To minimize the chance of the crystals hitting the wall, the flow in the chamber must be steady, axisymmetrical, and without recirculation in the vicinity of the crystal. We have performed experiments to determine flow rates, tube diameters, and angles of expansion necessary to suspend the crystals. A variety of small expansion chambers were used in these tests, the upper, larger diameters varied from 5 mm to 26 mm, the lower, smaller diameters from 2.5 mm to 4 mm, and the angles of expansion varied from 5 to 30°.

The onset of recirculation corresponds directly to a "bouncing" motion of the particle resulting in repeated contact with the chamber wall. In all the chambers, recirculation occurred in the flow rate range of 5-8 ml/min. These rates corresponded to the angle of expansion, larger angles showing recirculation at lower velocities, independent of the entering tube diameter. The optimal chamber dimensions resulting from these experimental studies are given in fig. 1. The transition from 3 mm to 10 mm in diameter, with a maximum 7° angle of expansion produces a more than 10-fold variation of velocity in the chamber and minimizes recirculation. With this chamber, particles in the size range of most interest for protein crystallization (0.4-1 mm) were suspended in the velocity range of 0.5-1.5 cm/s (based on the 3 mm part of the chamber). This velocity was then used as part of the design criteria for the thermosyphon.

2.3 Circulation Rates and the Design of the Thermosyphon

The design of the thermosyphon entails many factors. The flow rate is of primary concern. As discussed above, the narrowest part of the expansion chamber requires a flow velocity large enough to suspend a crystal of the final desired size. The temperature distribution in the thermosyphon must be such that nowhere the working limit of the solution is exceeded, the appropriate temperature for growth in the expansion chamber is provided, and nucleation elsewhere within the apparatus is reduced. The design must also minimize the total volume of solution and, thus, the amount of protein used. In general, larger diameter tubes decrease the fluid friction and increase the flow velocities at a given ΔT , but this increases the amount of fluid required in the apparatus. Another important consideration is to avoid the flow instabilities associated with thermosyphons [5-10] which are generally more prevalent when using large tubes at high heating rates.

The majority of theoretical and experimental analyses that deal with thermosyphons use very simplified geometries. There is a great deal of theoretical and experimental work on the "closed loop toroidal thermosyphon" [7-10] which, although not directly applicable to this more complex geometry, gave useful insight and guidance. Relations from Creveling et al. [7] provided an initial estimate that a tube diameter of 10 mm would be required for the desired flow velocity and this was later refined to 6 mm through experimental tests with thermosyphons. In light of these results, a thermosyphon crystal growth apparatus was constructed with 6 mm ID tubing for the majority of its length.

The crystal growth apparatus is shown in fig. 2. A concentric cooling jacket surrounds the right side of the loop, while the left side is heated by windings of copper-constantan wire connected to a controlled current supply. The port at the top is for filling the apparatus, inserting a thermistor to measure the maximum temperature, T_h , and for the addition of precipitants, pH buffers, and seed crystals or nuclei. The port at the bottom of the apparatus allows removal of crystals during operation and facilitates draining. The total volume of the apparatus is 20 ml.

The apparatus was designed for crystallization of materials having normal dependence of solubility on temperature, with the growth (expansion) chamber at the bottom of the heated section. The lower bend and the section entering the growth chamber are made from 3 mm ID tubing. This creates a localized higher velocity to aid the suspension of the crystals. The lower part of the apparatus is insulated so that the solution temperature at the site of the suspended crystal is essentially the same as that leaving the bottom of the cooled section, T_c . Hence the highest supersaturation in the loop occurs at the crystal. The velocity is increased or decreased, respectively by increasing or decreasing the temperature difference between the two sides of the apparatus. The temperature stability at a point, measured by the T_h thermistor and by the stability of the cooling bath was approximately $\pm 0.1^\circ\text{C}$

To operate this apparatus efficiently, one must understand how the temperature distribution in this loop affects the velocity. This insight is also important for up- or down-scaling of the apparatus without relying on trial and error. Due to the limited applicability of existing thermosyphon models to predict the velocity as a function of temperature in our apparatus, a mathematical model was developed to explore different geometries with higher suspension velocities and smaller required solution volumes. The mathematical model is based on the following considerations. The buoyancy force is integrated around the loop to obtain the flow-driving pressure differential. For steady state flow this force must equal the overall frictional force acting in the opposite direction. The input parameters are the geometry (the length, diameter and positions of the four segments of the apparatus), the physical properties of the solution, and the temperatures at the top of the heating section and at the crystal. The resistance heating section is assumed to have a constant heat flux boundary condition over its entire length. The temperature

distribution in the cooling section depends on the velocity as well as the thermal diffusivity of the circulating solution. Since it is the temperature distribution that determines the buoyancy force which, in turn, drives the velocity, an iterative solution of the heat and momentum transport equations was required. Details of this model will be published elsewhere.

Velocities in the thermosyphon crystal growth apparatus were measured and compared to those predicted by this model; see fig. 3. Note that the velocities are average velocities based on a 6 mm diameter tube. The velocities in the expansion chamber vary from 4 times these values (in the lower 3 mm part) to 0.36 times this value (in the upper 10 mm part). We see that the model can be used to predict the velocity with reasonable accuracy. The difference is most likely due to heat transferred to the expansion chamber from the ambient, which is neglected in the model. Since there are no empirical "fitting" parameters in this model, we feel confident that it can also be used to predict velocities in apparatuses of different geometry and size, as well as for solutions with different physical properties. Results from this model were used extensively for guidance during the crystal growth runs discussed below and for design of a smaller version of the apparatus (containing 6 ml) which is now under test.

For applications it is useful to note that the decreasing slope in fig. 3 is due to changes of the temperature distribution in the cold leg of the loop as the velocity is increased. The thermal entrance length in the cooled section increases with increasing velocity, thus reducing the overall buoyancy force. If the tube were very small in diameter, the thermal diffusivity very high, or the velocity very low, the temperature of the solution entering the cooled tube would quickly (i.e. after a short distance) reach the temperature of the wall, T_w . Consequently, many previous thermosyphon models are based on the assumption that the fluid in the entire cold section is at T_w . In the present model, however, full account is made of the developing temperature in the cold section, without assuming that T_w is reached at the sections end.

The effect of tube diameter on the solution velocity is complicated. Figure 4 shows the velocity as a function of tube diameter for three different values of $\Delta T = T_h - T_c$, the temperature difference between the hot and cold sides of the apparatus. The maximum arises from a combination of two opposing phenomena. For small tubes the viscous forces dominate and the corresponding drag reduces the velocity. For large tubes the thermal entrance length is longer and the effect discussed above becomes significant. Note that the curve for $\Delta T = 30^\circ\text{C}$ (a reasonable value for protein solutions) has its maximum near 6 mm, the size used in most of the loop in our crystal growth apparatus.

3. Crystallization Results

3.1 Operating procedures

Two inorganic systems (NaCl and $\text{AlK}(\text{SO}_4)_2$) were used to study the characteristics of the apparatus and to develop an "operating procedure" for startup, initiation of growth, and continued growth to the desired size. Several schemes were tried with the most successful one as follows. In this description, T_h , T_c , and ΔT are as defined above and T_s is the temperature at which the solution is saturated.

- 1) Set $\Delta T = 3^\circ\text{C}$ with both T_h and T_c , exceeding T_s . The flow in the loop recirculates at a low velocity and any nuclei or crystallites are dissolved.
- 2) Keeping $\Delta T \approx 3^\circ\text{C}$, lower both temperatures until $T_h < T_s$. The solution is now supersaturated but not enough to induce spontaneous nucleation.
- 3) Inject a small amount ($<0.05\text{ml}$) of saturated solution containing seed crystals. 1-10 mm crystals were used, but the size is not critical. These crystals are so small that they travel with the fluid around the loop while they are slowly growing.
- 4) When one or more crystals grow large enough to be trapped in the low velocity section of the growth chamber (typical size is 0.03 mm), increase T_c to the desired growth temperature keeping $\Delta T \approx 3^\circ\text{C}$. Since T_h is now larger than T_s , crystals which flow through the growth chamber are dissolved in the heated section.
- 5) Increasing the ΔT speeds the flow and sweeps the smaller crystals up into the heated section where they are dissolved. Decreasing the ΔT reduces the velocity to let the larger crystals settle down to the lower port where they are removed. This method was used to eliminate all but one crystal.
- 6) As the crystal in the chamber grows, it will gradually position itself lower in the expansion section where the velocities are higher. As the crystal continues to grow, T_h is increased to increase the velocity. At these higher velocities, the temperature of the solution reaching the crystal is not that of the cooling jacket. With results from the mathematical model for guidance, the cooling jacket temperature is lowered to maintain supersaturation at the crystal.
- 7) When the crystal has grown to the desired size, T_h is lowered, reducing the velocity, and the crystal sinks into the removal port. The crystal is then removed through a closely space pinch clamp assembly. This removal requires the drainage of only 0.04 to 0.1 ml.

Crystals of NaCl and $\text{AlK}(\text{SO}_4)_2$ were grown to 0.2 mm and 0.4 mm respectively. In light of the high relative density differences of these systems ($\rho_{\text{solid}}/\rho_{\text{solution}} = 1.8$ for NaCl and 1.35

for $\text{AlK}(\text{SO}_4)_2$ compared to that for protein systems (≈ 1.17 for lysozyme), these results were very promising. During these runs, it was discovered that a very small angle of inclination of the expansion chamber can cause a "bobbing" of the crystal and contact with the wall.

A small modification of the operating procedure allows for in situ nucleation. At step 2, both temperatures are lowered further to increase the supersaturation sufficiently for spontaneous nucleation. These nuclei grow while they circulate throughout the loop and are then trapped as before in step 4.

3.2 Tetragonal Lysozyme

First, a series of experiments were performed to grow tetragonal lysozyme crystals from nuclei formed in situ. The solution compositions ranged from 40 to 80 mg/ml lysozyme, 2 to 4 weight percent NaCl and were held at pH 4.5 with a 0.05 M acetate buffer. The temperatures in the apparatus ranged from 0 to 35°C, with the temperature for nucleation and or growth always below 25°C. These conditions favor the growth of the tetragonal form of lysozyme [11]. The supersaturation required for nucleation and growth was attained either via addition of NaCl (acting as a precipitating agent), or by temperature changes, or by combinations of both.

Nucleation occurred and crystallites were trapped in the expansion chamber. The crystallites had a very narrow size distribution, so the methods discussed above for reducing the number of crystals were not as successful as for the inorganic crystals. Each of the experiments took at least a week, due to the slow growth rates of lysozyme. The largest crystals grown were less than 0.1 mm and did not continue to grow even under supersaturation conditions which produced continued nucleation. Microscopic examination showed that the crystallites lacked well defined facets.

During these experiments we found that it took 2-3 weeks for any noticeable denaturization of the protein to occur in the form of a thin "haze" on the inner glass surfaces and some cloudiness of the solution. It was suspected that this was not the cause for the growth cessation of the crystallites. This was confirmed when solutions which had been circulating for more than three weeks grew large crystals (on the walls) when the circulation was stopped and the apparatus held at a constant temperature.

Next a series of experiments were done attempting continued growth of introduced tetragonal lysozyme crystal seeds. The seeds (0.03 to 0.5 mm) were produced in standing or hanging drops and were transferred to the thermosyphon via an Eppendorf pipet. The solutions used in these experiments had compositions which produce growth of lysozyme crystals in batch systems without causing spontaneous nucleation. During transfer of the seeds to the thermosyphon, the apparatus was held at a uniform, ambient temperature with no circulation. The temperature in the thermosyphon was then slowly changed to the desired operating conditions (over a period of hours) to start the flow and suspend the crystal. There was no measurable growth of the

suspended seeds during the time that the stagnant controls showed significant growth (see below). Experiments varied from 5 to 20 days. When the supersaturation was increased by lowering the temperature or addition of NaCl, there still was no growth and the facets of the seeds became "frosted". Two possible reasons for this behavior are:

1) Kinetic; due to the repeated heating and cooling the solution undergoes as it circulates. It has been speculated that lysozyme growth units are larger than monomers and, hence, there might be some "preclustering" necessary before attachment. On the other hand, there may be a conformational change in the molecule itself as it passes through the heated section. If the kinetics of this preclustering and/or conformational changes are slow, the proper growth units may not be available at the crystal beyond a certain flow velocity, i.e. at too frequent temperature cycling of the solution.

2) Mechanical; due to the crystal being suspended by the drag forces of the fluid around it. It is possible that the shear forces on the surface of the crystal hinder the attachment of the growth units.

The second reason would have very important implications for the growth of protein crystals in space as well as on earth. One of the main reasons cited for growing crystals in space is the reduction of bouyancy induced convection. These thermosyphon growth experiments appear to indicate that convection has an adverse affect and can cause "growth cessation." This observation corroborates earlier work by Pusey et al. [12], which showed that the growth rate of tetragonal lysozyme crystals subjected to a forced flow of solution decreased significantly after 1/2 to 2 hours of growth.

A set of stagnant control experiments were performed concurrently with the thermosyphon runs. Various constant temperatures were used with the same solution and seeded at the same time with seeds from the same sandwich (or hanging) drop. These control experiments produced important results of their own and were essential for developing succesful seed transfer techniques. It was found that if a seed crystal undergoes a sudden temperature change of more than a few degrees during the transfer, it will not grow thereafter. Additionally, when the solution the seed was transferred to had a different (by 0.003 gm/ml or more) salt concentration, no growth occurred. Hence, we developed the following transfer technique. 1) Nucleate and grow seed crystals in a hanging drop. 2) Move the cover slip with the hanging drop to a new reservoir which has the (lower) NaCl concentration of the solution in the thermosyphon. 3) Allow 2 days for equilibration before the crystal is transferred with a pipet. In contrast to the thermosyphon runs, tetragonal lysozyme seed crystals transferred to temperature controlled batch cells with this technique showed uninhibited growth.

3.3 Orthorhombic Lysozyme

Similar tests were done under conditions favorable for the growth of orthorhombic lysozyme. In contrast to the results obtained with the tetragonal form, there was no cessation of growth. After in-situ nucleation, and without any change of conditions (temperature or concentration) a single crystal became visible in the expansion chamber. As it grew, T_h was raised to increase the velocity and to keep the crystallite suspended. It grew to a size of $1.5 \times 0.5 \times 0.2$ mm before it was removed. At this time a few other, smaller, crystals had appeared and were growing. These were also removed successfully after growth to their suspension limit. Similar results were achieved during experimental runs utilizing seed crystals.

4. Summary and Conclusions

A solution crystal growth apparatus was designed based on fluid dynamic considerations, and applied to the growth of protein crystals to avoid contact with container walls, dialysis membranes or liquid-vapor interfaces. The crystals are suspended during growth in an upflow of supersaturated solution provided by natural convection in a closed loop thermosyphon. This buoyancy-driven flow alleviates the possible damage of protein solutions due to the shear field of mechanical pumps. While the crystal remains suspended in a fixed position within the expansion chamber at a constant temperature (controlled to within 0.1°C), the solution is thermally cycled as it recirculates throughout the apparatus. This leads to the dissolution of new nuclei, thus excluding the mechanical interference of numerous crystals growing concurrently as in other protein growth techniques.

Whereas orthorhombic lysozyme grew up to the suspension limit of this apparatus of 1.5 mm, tetragonal lysozyme growth ceased at about 0.1 mm even at supersaturations where concurrent nucleation became pronounced. At this point it is not clear whether this growth cessation is of thermal or mechanical origin. We speculate that the reason that the growth of orthorhombic crystals is not inhibited is that the ratio of the growth unit's attachment force to its size may be larger. These results are particularly interesting in terms of the recently found significant improvement of the structural quality of various protein crystals grown under low gravity conditions in the Spacelab [13]. One can speculate that the shear forces experienced by crystals during growth on Earth, in the more traditional techniques due to solutal convection and in our apparatus due to the suspension flow, can be detrimental to the proper attachment of "building blocks", or growth units. This speculation becomes reasonable, considering the low bond strengths involved in protein crystallization and the large dimensions of the growth units, in particular if they consist of multimolecular clusters [14].

The applicability of our technique to other proteins is likely limited to mechanically and configurationally relatively stable species. In addition, limitations arise from the relatively large

amount of solution required (≈ 6 mls). However, as a scaling analysis indicates, the technique may well be suited to the growth of centimeter sizes of small-molecule materials, which, however, will require mechanical pumping to obtain the high suspension velocities required. The pumping of such shear-insensitive solutions should cause no damage to the solute. Optimal stirring conditions (that minimize the inclusion of mother liquor) and the absence of mechanical seed suspension devices are particularly attractive features of the flow-suspension crystal growth technique.

5. Acknowledgements

The authors are grateful for the support provided by the National Aeronautics and Space Administration under Grants No. NAG8-098 and NAG8-711. This research has also been supported by the State of Alabama through the Center for Microgravity and Materials Research at the University of Alabama in Huntsville.

6. References

- [1] G. G. Stokes, *Trans. Cam. Phil. Soc.* **9** (1851) 8.
- [2] L. Schiller and A. Nauman, *Z. Ver. deut. Ing.* **77** (1933) 318.
- [3] H. A. Becker, *Can. J. Chem. Eng.*, **37** (1959) 85.
- [4] R. Ladenburg, *Ann. Phys.* **23** (1907) 447.
- [5] Y. Zvirin, *Nucl. Eng. Design* **67** (1981) 203.
- [6] A. Mertol and R. Greif, *Natural Convection: Fundamentals and Applications*. S. Kakac, W. Aung, and R. Viskanta (ed.) (Hemisphere, New York 1985) 1033.
- [7] H. F. Creveling, J. F. DePaz, J. Y. Baladi, and R. J. Schoenhals, *J. Fluid Mech.* **67** (1975) 65.
- [8] P. S. Damerell and R. J. Schoenhals, *J. Heat Transfer* **101** (1979) 672.
- [9] R. Grief, Y. Zvirin, and A. Mertol, *J. Heat Transfer* **101** (1979) 684.
- [10] J. E. Hart, *J. Heat Transfer* **107** (1985) 839.
- [11] P. Jollés and J. Berthou, *FEBS Letters*, **23** (1972) 21.

- [12] M. Pusey, *J. Crystal Growth*, **90** (1988) 105.
- [13] L. DeLucas et al., (submitted to *Science*)
- [14] M. Pusey, (this proceedings)

FIGURE CAPTIONS

- Figure 1. Growth and expansion chamber.
- Figure 2. Thermosyphon crystal growth apparatus
- Figure 3. Velocity in the thermosyphon as a function of the temperature difference between the heated section and the cooling jacket temperature. Comparison of experimental values (circles) with model calculations (line).
- Figure 4. Model calculations for the average solution velocity in the thermosyphon as a function of tube diameter for various temperature differences.

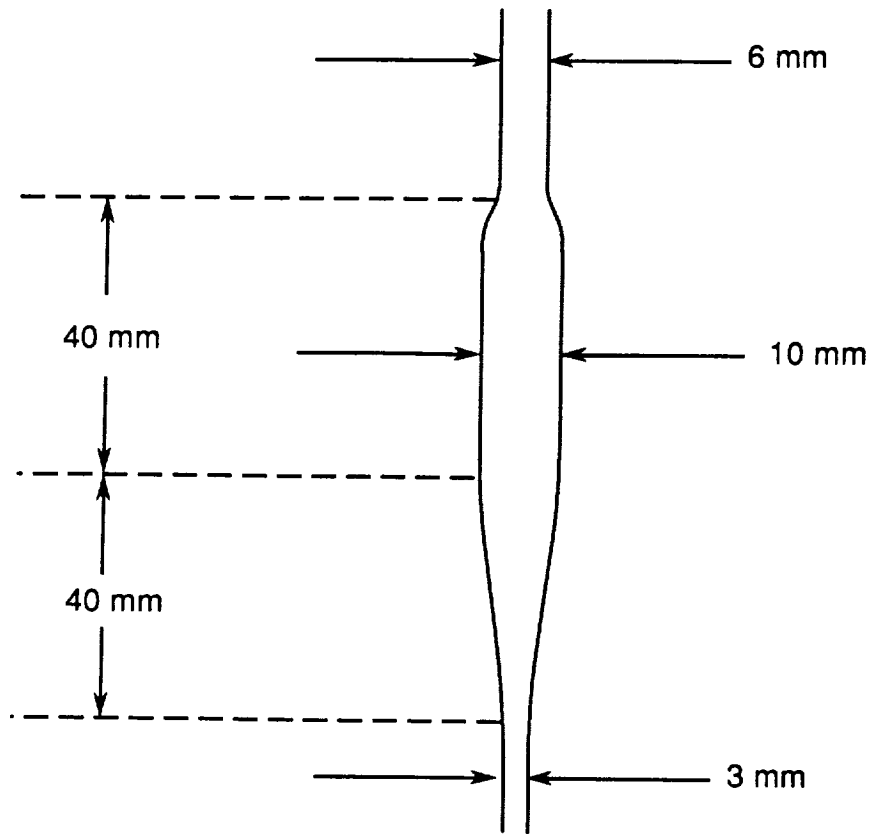


figure 1

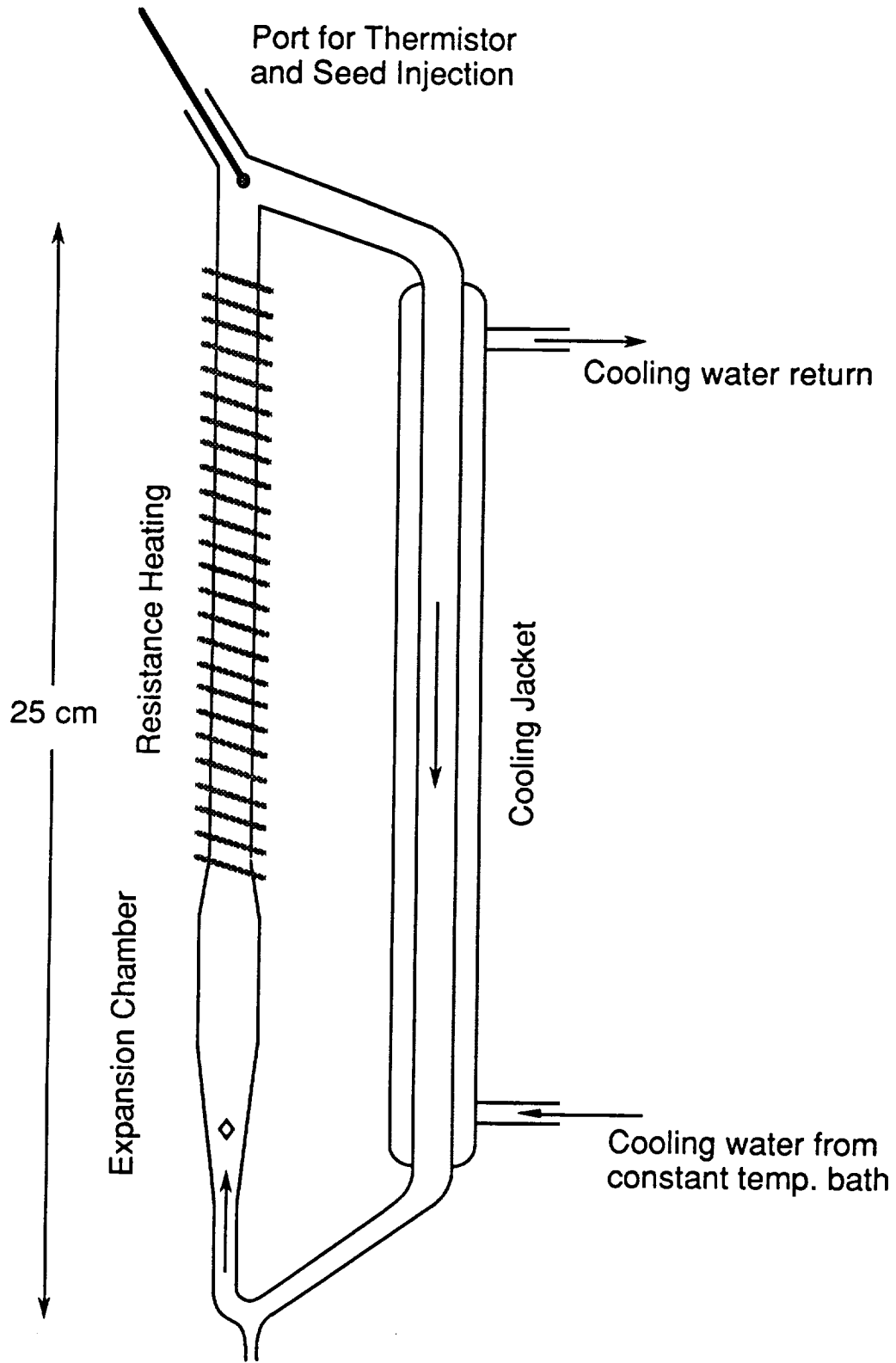


figure 2

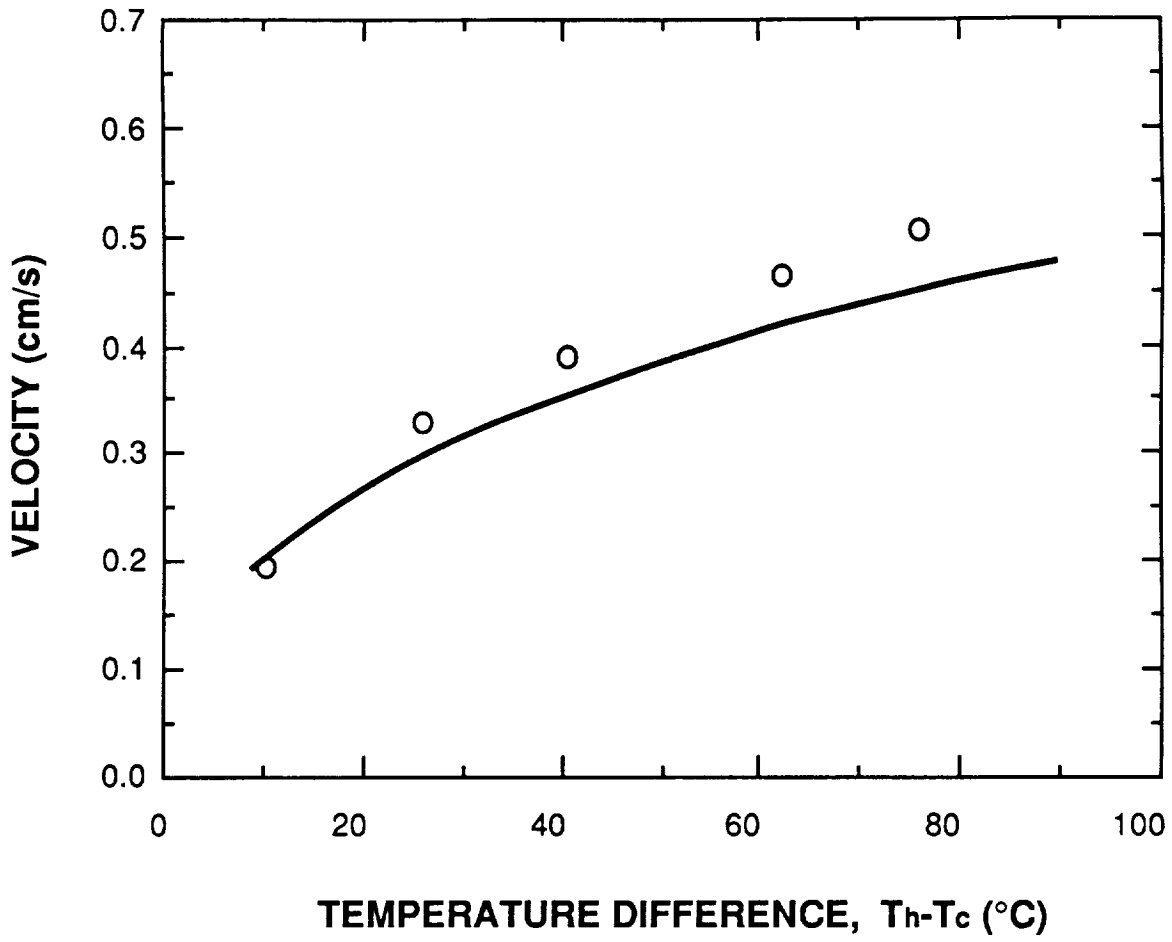


figure 3

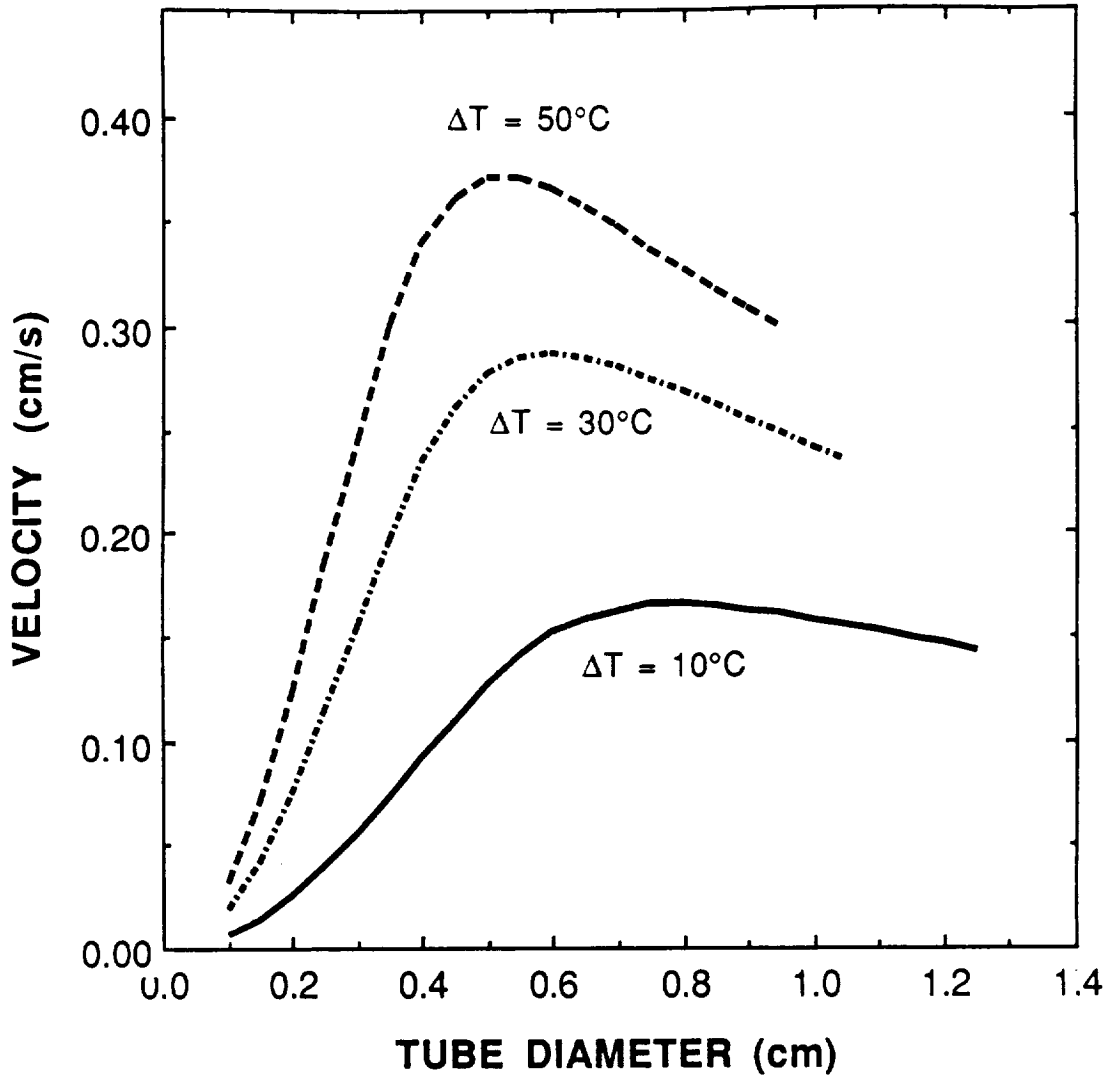


figure 4

A GENERAL METHOD FOR CALCULATING VELOCITIES AND HEAT TRANSFER IN CLOSED LOOP NATURAL CONVECTION SYSTEMS

Thomas A. Nyce† and Franz Rosenberger‡*

ABSTRACT

A relatively simple-to-use method is presented for the calculation of velocities and heat transfer in closed loop natural convection systems such as solar water heaters and nuclear reactor cooling systems during shutdown. The method can accommodate systems that consist of sections with different diameters, lengths, friction factors and heat transfer boundary conditions. After a general description of the method it is applied specifically to natural convection in a tilted square loop. Good agreement of the model results with experimental data of Acosta et al. (Wärme Stoffübertragung 21 (1987) 269) is obtained.

† Research Scientist, Center for Microgravity and Materials Research
University of Alabama in Huntsville, Huntsville, Alabama 35899

‡ Director and Professor, Center for Microgravity and Materials
Research, University of Alabama in Huntsville, Huntsville, Alabama
35899

* To whom correspondence should be addressed.

NOMENCLATURE

C_p	heat capacity of fluid (J/kg•°C)
D	diameter of tube (m)
g	magnitude of gravity vector (m/s ²)
k	thermal conductivity of fluid (W/m ² °C)
L	total length of the loop (m)
p	pressure (N/m ²)
Q	total heat input (W)
r	tube radius (m)
s	distance in flow direction (m/s)
T	temperature (°C)
T_w	wall temperature of cooled section (°C)
U	cross-sectional average velocity (m/s)
x^+	dimensionless distance —
α	tilt angle of square loop (degrees)
β	coefficient of thermal expansion (°C ⁻¹)
ϕ_m	mixed mean temperature —
κ	thermal diffusivity of fluid (m ² /s)
μ	dynamic viscosity (kg/m•s)
τ_w	fluid shear stress at the wall (N/m ²)
ρ	fluid density (kg/m ³)
θ	angle between flow direction and gravity vector (degrees)

1. Introduction

Natural convection loops encompass a broad range of applications, such as in nuclear reactor cooling, geothermal energy utilization, and solar water heaters. A recent review [1] discusses a number of representative works and emphasizes the importance of this diverse area of research.

Most theoretical investigations of convection loops deal with a toroidal thermosyphon. A primary goal has been to develop an understanding of the flow and heat transfer in this relatively simple geometry which then could be applied to the typically more complicated geometries and boundary conditions of most practical applications. Yet, as the understanding of toroidal thermosyphons progressed, it has become clear that the flow and heat transfer in these systems is anything but simple. Unsteady and even three-dimensional flows have been experimentally verified [2-4] while mathematical models have become correspondingly complex and difficult to solve. Furthermore, as the models became more specific to the toroidal thermosyphon, the results increasingly lost their utility to the designer of more useful thermosyphons.

The mathematical model presented here is a relatively simple-to-use tool for predicting flow rates and heat transfer rates in natural convection loops. In the derivation, the general features of the method are emphasized so that it can be applied to a variety of geometries. The method is best suited for natural convection loops which can be considered as a sequence of individual "legs" or sections, each with different heat transfer boundary conditions and with different friction factors. Each leg is then treated individually, based on a separate equation for the energy balance. The sections are then dealt with sequentially. For each section, there is an inflow velocity and temperature which must correspond to those at the

outflow of the upstream section. The physical (size and shape) and thermal boundary conditions of the section are then used to calculate the outflow velocity and temperature which are the input parameters for the next section. The calculations can be analytical, numerical or be based on empirical correlations. This process is continued around the loop. All that needs to be known for each section to calculate steady flows and the heat thus transferred are the average density of the fluid as a function of height and the frictional forces as a function of velocity. The method is particularly advantageous when certain assumptions are valid over some sections of the loop but not others.

2. Mathematical Model

2.1 The General Model

Let a natural convection loop of length L have n segments. The distance s measured along the loop (from an arbitrarily chosen junction of two segments) to the end of the i th segment is s_i . The lengths of the n segments are thus $s_1, s_2-s_1, \dots, s_n-s_{n-1}$. The steady state equations for conservation of mass and momentum are

$$\frac{\partial(\rho U)}{\partial s} = 0, \quad (1)$$

$$\frac{\partial(\rho U^2)}{\partial s} = -\frac{\partial p}{\partial s} - \rho g \cos\theta - \frac{2}{r} \tau_w, \quad (2)$$

where U is the average cross sectional velocity, θ is the angle between the flow direction and the gravity vector, and r is the inner radius of the tube. If we assume steady state conditions, (1) indicates that the mass flux ρU is

constant along the loop. Assuming $\rho = \rho_0(1 - \beta(T - T_0))$ and integrating (2) around the length of the loop gives

$$-\rho_0 \beta g \int_0^L T \cos\theta \, ds + 2 \int_0^L \frac{\tau_w}{r} \, ds = 0. \quad (3)$$

To allow for changing boundary conditions along the loop, the integrals are carried out piecewise; the pieces corresponding to the sections of the apparatus.

$$-\rho_0 \beta g \sum_{i=0}^{n-1} \int_{s_i}^{s_{i+1}} T \cos\theta \, ds = 2 \left(\int_0^{s_1} \frac{\tau_w}{r} \, ds + \sum_{i=0}^{n-1} \int_{s_i}^{s_{i+1}} \frac{\tau_w}{r} \, ds \right) \quad (4)$$

This equation represents a balance of the buoyancy forces (left side) and the frictional forces (right side) required for steady state circulation. Both, the temperature distribution in the fluid needed for the evaluation of the left side of (4), and the distribution of frictional forces needed for solving the right side of (4) require knowledge of the velocity distribution around the loop. In the following example, this method is applied to natural convection in a tilted square loop.

2.1 Application to a Square Thermosyphon Loop with Tilt

In the absence of experimental results for a well characterized, more complicated natural connection loop, we will test our method against data obtained by Acosta et al. [5]. A schematic representation of their apparatus is given in Figure 1. There are four legs to this loop, which we will label sections 1-4 counterclockwise starting with the bottom leg. Section 1 is heated electrically and section 3 is cooled with a coaxial cylindrical heat

exchanger. The right vertical leg is an insulated PVC tube while the left side is an uninsulated glass tube. The apparatus can be tilted by α degrees, measured as rotation counterclockwise.

First, equations describing the temperature distribution are developed for each of the sections. Second, equations relating the temperatures at the junctions of the four sections are obtained. For section 1, we assume a uniform heat flux. This means that, for $0 \leq s \leq s_1$, the average temperature varies linearly with distance through the tube according to

$$T = T_0 + (T_1 - T_0) \left(\frac{s}{s_1} \right), \quad (5)$$

where T_0 and T_1 , respectively, are the temperature of the fluid entering and leaving section 1. An energy balance over the entire section yields

$$T_1 = \frac{Q}{U\rho C_p \pi r} + T_0, \quad (6)$$

where Q is the total heat input over section 1.

We assume that section 2 is adiabatic and the temperature is constant at T_1 and thus, the exiting temperature,

$$T_2 = T_1. \quad (7)$$

For section 3, the cooled top section of the loop, the fluid's temperature is a function of distance through the section, the temperature of the cooling wall T_w , and the thermal diffusivity of the solution $\kappa = k/\rho C_p$. The solution of the energy equation for the thermal entry region of a tube with constant surface temperature is given in [6]. This series solution can be represented by

$$\phi_m = 8 \sum \frac{G_n}{\lambda_n^2} \exp(-\lambda_n^2 x^+), \quad (8)$$

where the G_n and λ_n^2 are given in [7], x^+ is the dimensionless distance defined as $x^+=2\kappa(s-s_2)/(UD^2)$, and ϕ_m is the mixed mean temperature defined in our case as

$$\phi_m = \frac{T - T_w}{T_2 - T_w},$$

with T_2 the temperature of the fluid entering section 3. Setting $s=s_3$ in (8) gives ϕ and thus T_3 at the exit of section 3.

Section 4 is not insulated and there may be heat transfer to or from the environment. This heat transfer is proportional to the convective heat transfer coefficient and the difference between the fluid temperature and the ambient. Acosta et al [5] report only the temperature difference across the heated section. However, from their results it can be deduced that the heat lost in this section is much less than the heat transferred in sections 1 and 3 and thus we will neglect it and assume an adiabatic condition as for section 2. This means the temperature in section 4 is constant at T_3 and the exiting temperature,

$$T_0 = T_3. \quad (9)$$

Now, the $\int T \cos\theta$ terms for equation (4) must be developed. For section 1, (6) is used to give

$$\int_0^{s_1} T \cos\theta ds = \int_0^{s_1} T (-\sin\alpha) ds = -\frac{s_1}{2}(T_1 + T_0) \sin\alpha. \quad (10)$$

For section 2, the temperature is constant at T_1 , therefore

$$\int_{s_1}^{s_2} T \cos\theta dS = \int_{s_1}^{s_2} T_1(-\cos\alpha) ds = -T_1 \cos\alpha (s_2 - s_1). \quad (11)$$

For section 3, (9) is integrated and the definition of ϕ is used to give

$$\int_{s_2}^{s_3} T \cos\theta \, ds = \sin\alpha \left[T_w(s_3 - s_2) + (T_2 - T_w) \sum_0^n \frac{4G_n U D^2}{\lambda_n^4 \alpha} \left(1 - \exp\left(-\frac{\lambda_n^2 2\kappa}{U D^2}(s_3 - s_2)\right) \right) \right]. \quad (12)$$

Section 4 has a constant temperature T_0 , and thus

$$\int_{s_3}^{s_4} T \cos\theta \, ds = \int_{s_3}^L \cos\alpha \, ds = T_0 \cos\alpha (L - s_3). \quad (13)$$

Next, the frictional forces must be calculated as a function of the average velocity U . In Acosta's apparatus the diameter of the tubes is constant. If we assume fully developed laminar flow throughout the tubes we can approximate the frictional forces in the loop by

$$2 \int_0^L \frac{\tau_w}{r} \, ds = \frac{32U\mu L}{D^2} + 4F_{\text{elbow}}, \quad (14)$$

where F_{elbow} is the pressure drop due to a 90° elbow and is a function of the velocity U . We have calculated the elbow friction with relations given by Kitteredge and Rowley [8].

Substituting $T_1=T_2$ into (12) and substituting (11-14) into (3) gives

$$-\rho_0 \beta g \left[\sin\alpha \left(f(U, T_1) - \frac{s_1}{2}(T_1 + T_0) \right) + \cos\alpha (T_0(L - s_3) - T_1(s_2 - s_1)) \right] - \frac{32U\mu L}{D^2} + 4F_{\text{elbow}} = 0. \quad (15)$$

For convenience, we have represented the right hand side of (12) by $\sin\alpha f(U, T_1)$. Note that the unknowns in (15) are U , T_0 , and T_1 , but T_0 and T_1 can be solved for as functions of U . Substitution of these $T_0(U)$ and $T_1(U)$ back into (15) gives an equation in U alone. To do this (7) and (9) are

substituted into (8) and, subsequently, (5) and (8) are combined and rearranged to give

$$T_0 = \frac{\frac{Q}{U\rho C_p \pi r} \phi_{s3} + T_w}{1 - \phi_{s3}}, \quad (16)$$

where ϕ_{s3} is obtained from (8) with $s=s_3$. $T_1(U)$ is then calculated from equation (5). U cannot be solved for explicitly from the resulting (15), but any of a variety of iteration methods (bisection, secant, Newton-Raphson etc.) can be used to solve for it.

Recognizing that (15) is composed of two parts, the buoyancy forces which drive the flow and the frictional forces which impede it, means that an iteration method which is more closely tied to the physics of the problem can be developed. Assuming a given volumetric flow rate around the loop, the temperature distributions and, thus, the buoyancy forces can be calculated. The velocity cannot be solved for explicitly from the relations for elbow friction and thus this term is calculated with using U_1 and grouped with the buoyancy terms. A new velocity is then calculated by rearranging (15) as

$$U_{i+1} = \frac{D^2}{32\mu L} \left[\rho_0 \beta g \left[\sin\alpha \left(f(U_i, T_1) - \frac{s_1(T_1 + T_0)}{2} \right) + \right. \right. \\ \left. \left. + \cos\alpha (T_0(L - s_3) - T_1(s_2 - s_1)) \right] + 4F_{\text{elbow}} \right]. \quad (17)$$

This new velocity is then used as a "next guess" for the buoyancy force calculation and the process is repeated until convergence is obtained. The advantage of this type of iteration is that it can only converge to physical solutions. This is important because there clearly are solutions to (15) which are unstable to any perturbation and are thus physically unrealistic.

An example is the zero velocity solution for zero tilt angle. For this example, the buoyancy forces are zero because the temperature profile is symmetric about the vertical center plane and the frictional forces are also zero, satisfying (15). In the experimental situation a slight asymmetry in the boundary conditions would lead to flow which would lead to further asymmetry, driving an increasing flow rate until limited by the increasing frictional forces. We should expect steady flows only in velocity ranges where the buoyancy forces decrease with increasing flow rate and frictional forces increase with increasing flow rate. Under these conditions, during the above iteration process, if the calculated buoyancy forces are greater than the frictional forces, an increase in the assumed velocity (via (17)) will bring the two forces closer in balance. This mathematical process is similar to the physical process of a natural convection loop dynamically approaching a steady state velocity under a fixed set of temperature boundary conditions.

3. Results

The physical parameters of the apparatus were obtained from [5]. The square loop was 50 cm on a side with tubes of 2 cm diameter. Velocities were calculated from (15) with the given heating rate of 0.83 Watt and via the "physical" iteration scheme described above. In Figure 2 we compare the results of the calculation with the experimental results of [5]. The agreement is quite good considering that the calculation uses no "experimentally derived" parameters. No steady state solutions could be obtained for tilt angles less than -116° or greater than 116° .

The largest differences between model results and experimental data are at high flow rates. For these conditions, probably the worst model assumptions are in the calculation of the frictional forces. The friction

depends on the kind of elbow used (which wasn't specified in [5]) and becomes a larger percentage of the total friction as the velocity increases. To illustrate this, we have also plotted in Fig. 2 the velocities obtained without the elbow friction terms in (15). Furthermore, the friction in the straight tubes was calculated based on fully developed flow, which certainly does not apply throughout the loop. Improved agreement at high heating rates, and thus higher flow rates, could possibly be obtained by using the friction of a hydrodynamically developing flow and empirical friction factors for the specific type of elbow used.

4. Summary and Conclusions

We have presented a general method for the calculation of flow velocities in natural convection loops that may consist of sections with largely differing geometrical and thermal boundary conditions. The sections are treated individually, requiring only relations for the pressure drop and temperature change as a function of flow rate, and, for non-horizontal sections, the average cross-sectional temperature as a function of height. Hence, variable tube diameters, sudden expansions or valves, and even non-cylindrical duct cross sections, such as corrugated, plate-type heat exchangers, can readily be incorporated into the model without detailed knowledge of the flow field in a specific section. Such cases cannot be described with a regular discretization approach. As an additional benefit, the friction and buoyancy contributions for each section can be retained in the model. This "intermediate" information gives insight into the physics of an apparatus and, thus, allows for better design optimization.

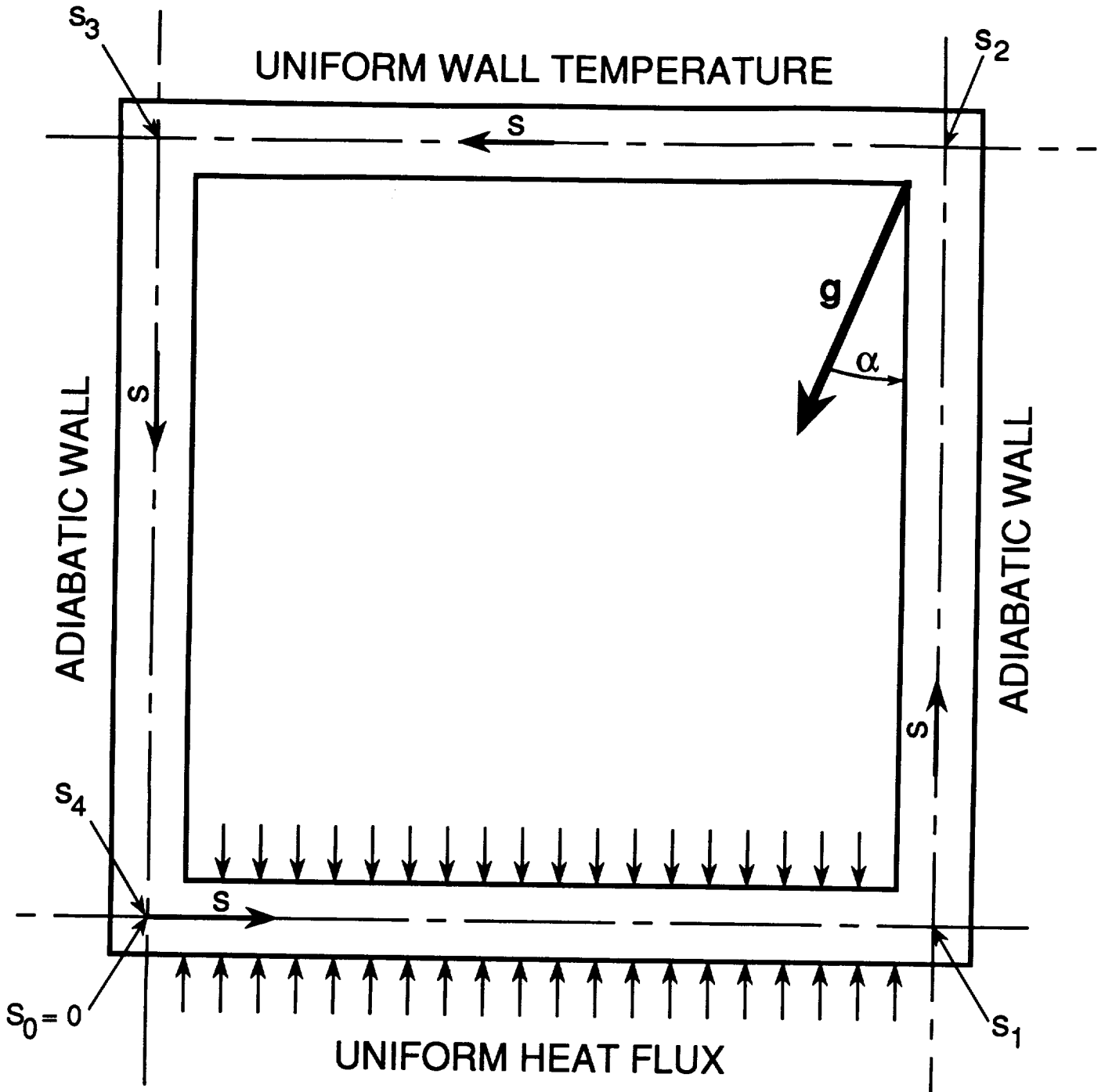
6. References

- [1] R. Greif, Natural circulation loops, *J. of Heat Transfer* **110**, 1243-1258 (1988).
- [2] H. F. Creveling, J. F. DePaz, J. Y. Baladi, and R. J. Schoenhals, Stability characteristics of a single-phase free convection loop. *J. Fluid Mech.* **67**, 65-84 (1975).
- [3] P. S. Damerell and R. J. Schoenhals, Flow in a toroidal thermosyphon with angular displacement of heated and cooled sections. *J. Heat Transfer* **101**, 672-676 (1979).
- [4] C. H. Stern, R. Greif, and J. A. C. Humphrey, An experimental study of natural convection in a toroidal loop. *J. Heat Transfer* **110**, 877-884 (1988).
- [5] R. Acosta, M. Sen, and E. Ramos, Single-phase natural circulation in a tilted square loop. *Wärme- und Stoffübertragung* **21**, 269-275 (1987).
- [6] W. M. Kays and M. E. Crawford, *Convective Heat and Mass Transfer*, McGraw Hill, New York, (1980).
- [7] J. R. Sellars, M. Tribus, and J. S. Klein, Heat transfer to laminar flow in a round tube or flat conduit - the Graetz problem extended. *Trans. ASME*, **78**, 441-448 (1956).
- [8] Kitteredge and Rowley, Resistance coefficients for laminar and turbulent flow through one-half-inch valves and fittings. *Trans. ASME* **79**, 1759-1766 (1957).

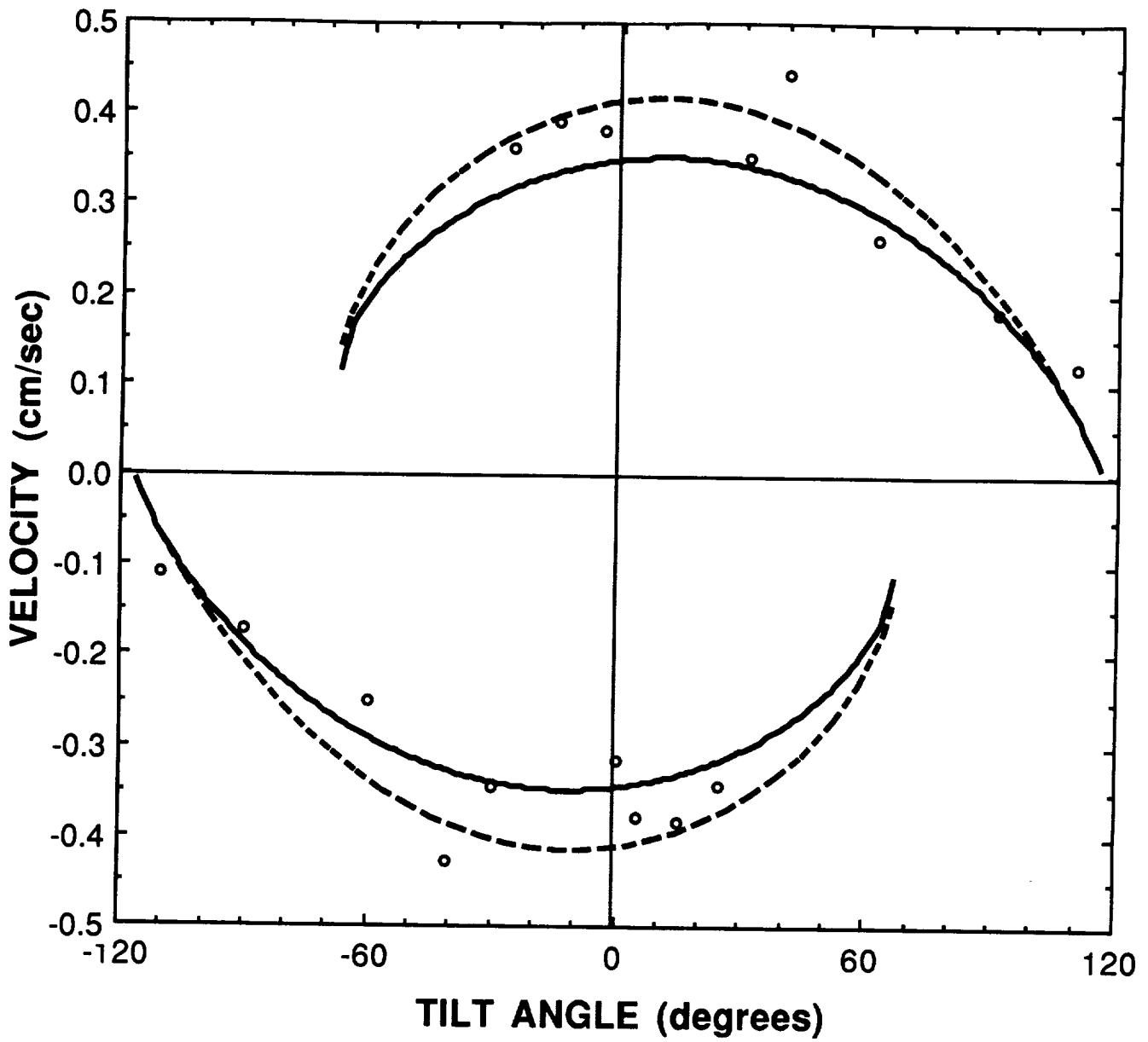
FIGURE CAPTIONS

Figure 1. Schematic of tilted square thermosyphon loop.

Figure 2. Velocity as a function of tilt angle in a tilted square thermosyphon loop. Model predictions with (solid line) and without (dashed line) friction in elbows. Experimental data (o) from Acosta et al. [5].



Nyce and Rosenberger
Figure 1



Nyce and Rosenberger
Figure 2